

Assessing subhalo finders in cosmological hydrodynamical simulations

Victor J. Forouhar Moreno^{1*}, John Helly², Rob McGibbon¹, Joop Schaye¹, Matthieu Schaller^{3,1},
Jiaxin Han^{4,5} and Roi Kugel¹.

¹*Leiden Observatory, Leiden University, PO Box 9513, NL-2300 RA Leiden, the Netherlands*

²*Institute for Computational Cosmology, Department of Physics, University of Durham, South Road, Durham, DH1 3LE, UK*

³*Lorentz Institute for Theoretical Physics, Leiden University, PO Box 9506, 2300 RA Leiden, the Netherlands*

⁴*Department of Astronomy, School of Physics and Astronomy, Shanghai Jiao Tong University, Shanghai 200240, PR China*

⁵*Shanghai Key Laboratory for Particle Physics and Cosmology, Shanghai 200240, China*

Accepted XXX. Received YYY; in original form ZZZ

ABSTRACT

Cosmological simulations are essential for inferring cosmological and galaxy population properties based on forward-modelling, but this typically requires finding the population of (sub)haloes and galaxies that they contain. The properties of said populations vary depending on the algorithm used to find them, which is concerning as it may bias key statistics. We compare how the predicted (sub)halo mass functions, satellite radial distributions and correlation functions vary across algorithms in the dark-matter-only and hydrodynamical versions of the FLAMINGO simulations. We test three representative approaches to finding subhaloes: grouping particles in configuration- (Subfind), phase- (ROCKSTAR and VELOCIRAPTOR) and history-space (HBT-HERONS). We also present HBT-HERONS, a new version of the HBT+ subhalo finder that improves the tracking of subhaloes. We find 10%-level differences in the M_{200c} mass function, reflecting different field halo definitions and occasional miscentering. The bound mass functions can differ by 75% at the high mass end, even when using the maximum circular velocity as a mass proxy. The number of well-resolved subhaloes differs by up to 20% near R_{200c} , reflecting differences in the assignment of mass to subhaloes and their identification. The predictions of different subhalo finders increasingly diverge towards the centres of the host haloes. The performance of most subhalo finders does not improve with the resolution of the simulation and is worse for hydrodynamical than for dark-matter-only simulations. We conclude that HBT-HERONS is the preferred choice of subhalo finder due to its low computational cost, self-consistently made and robust merger trees, and robust subhalo identification capabilities.

Key words: galaxies: haloes, dark matter, large-scale structure of Universe

1 INTRODUCTION

The formation of cosmic structure is driven by gravity, which amplifies small deviations from homogeneity in the early Universe. Overdense regions eventually undergo gravitational collapse, leading to the formation of dark matter (DM) haloes. This process is hierarchical in nature, as the smallest haloes form first, and subsequently grow through mass accretion and mergers with neighbouring ones. As the formation of galaxies is tied to the formation of dark matter haloes, galaxies trace the underlying distribution of matter in the Universe.

The initial distribution of matter in the Universe, as well as its subsequent evolution, depend on cosmological parameters and the nature of dark matter. The amplitude of density fluctuations depends on σ_8 . The subsequent growth of structure is further modulated by the relative amounts of matter and dark energy. As such, measuring the distribution, abundance and properties of structure in the Universe is an essential tool to study its cosmology.

In the past, this approach helped rule out hot models of dark matter (White et al. 1983), as well as hint at a non-zero cosmological constant (e.g. Efstathiou et al. 1990). Ongoing surveys aim to constrain

key cosmological parameters, such as the amplitude of power fluctuations (e.g. via weak lensing; Euclid Collaboration et al. 2024a), or the nature of dark matter (e.g. using Milky Way satellites; Drlica-Wagner et al. 2019). Making such cosmological inferences requires forward modelling the evolution of structure in the Universe under different sets of parameter choices. This in turn involves running cosmological simulations of increasingly large volumes and higher resolutions. However, simulations follow individual mass elements, rather than the conglomerate structures that they are a part of. As such, an important step in this process is finding where the haloes and the galaxies that they harbour are located.

Identifying (sub)haloes is non-trivial. They are found in a variety of environments and evolutionary stages, with some combinations being inherently more difficult to analyse than others. For instance, field haloes can be found with relative ease using the Friends-of-Friends (FoF) algorithm (e.g. Press & Davis 1982). This method links all particles within a threshold distance, typically chosen to be 0.2 of the mean interparticle separation. This roughly corresponds to an overdensity of 100 times the critical density of the universe (More et al. 2011).

Nonetheless, field haloes are often accreted by more massive ones and become satellite subhaloes. If this happens, the simple FoF algorithm is unable to distinguish the satellite from the host. This means

* E-mail: forouhar@strw.leidenuniv.nl

that additional steps are required to separate satellite subhaloes from the halo that hosts them. Not doing so would mean that only a subset of the total population of subhaloes in the Universe would be found.

Many algorithms have been developed with the aim of finding subhaloes. They primarily rely on segmenting particles within individual FoF groups into candidate subhaloes. As this can include chance groupings of particles due to discreteness noise, additional checks are done to clean catalogues from spurious subhaloes. For example, by requiring subhaloes to contain a minimum number or fraction of self-bound particles.

However, differences exist between the subhalo populations that subhalo finders identify. This can often be attributed to how they identify candidate subhaloes, as well as their definition of what a subhalo actually is. There are three main approaches in the literature. Configuration space finders rely on identifying density peaks (or overdensities) in the matter distribution, e.g. by kernel smoothing (SUBFIND; Springel et al. 2001, ADAPTAHOP; Aubert et al. 2004), adaptive mesh refinement (AHF; Gill et al. 2004; Knollmann & Knebe 2009), or hierarchical 3D FoF finding (HFoF; Klypin et al. 1999). Phase-space finders use the position and velocity of particles, such as by doing 6D FoF finding (ROCKSTAR; Behroozi et al. 2013a) or finding local peaks in spatial and velocity density (VELOCIRAPTOR; Elahi et al. 2011, 2019a). The additional information provided by the velocity of particles helps overcome several shortcomings of configuration space finders, such as when subhaloes spatially overlap but remain physically distinct entities (e.g. Behroozi et al. 2015).

The third approach is based on ‘history’-space, e.g. SURV (Giocoli et al. 2010), HBT (Han et al. 2012) and HBT+ (Han et al. 2018). The idea is to use information from previous outputs, as that way subhaloes can be first identified when it is easier to do so (e.g. before becoming satellites). The information is then used at later times, so that the algorithm does not have to disentangle the often complicated instantaneous distribution of particles. This alternative approach has been shown to improve the results of subhalo finders and the resulting merger trees (Chandro-Gómez et al. 2025), and has been gaining traction in recent years (e.g. Springel et al. 2021; Diemer et al. 2024; Mansfield et al. 2024).

Each type of subhalo finder has an associated drawback, which can be reflected in the properties of the subhalo population that they (do not) find. As mentioned before, density peak finders struggle to separate subhaloes that are close in space, such as when close pericentre passages or major mergers occur (e.g. Behroozi et al. 2015). Phase-space finders can also struggle to locate subhaloes that are severely tidally distorted (e.g. Diemer et al. 2024). Both cases of subhalo misidentification occur even when the number of particles sampling them is large, so the problem is not uniquely driven by a lack of resolution. For history-based finders, the need for a sufficient number of finely time-spaced outputs increases the storage requirements. This also means that the output strategy of simulations needs to be set ahead of time. Additionally, since the catalogues at later times depend on earlier ones, small errors in the tracing of subhaloes, or incorrect assumptions of how they evolve, may amplify over time. Lastly, current history based finders assume hierarchical structure formation, making it difficult to identify subhaloes that formed via fragmentation of a common progenitor, such as tidal dwarf galaxies.

Understanding how the choice of subhalo finder affects the subhalo population, and hence the predictions to which observations are compared, is essential in the era of precision cosmology. Previous studies have looked at how different subhalo finders perform in a range of idealised test cases, as well as zoom-in and cosmological simulations (e.g. Knebe et al. 2011; Onions et al. 2012; Behroozi

et al. 2015). The comparisons, which were based on only analysing the dark matter particles to find subhaloes, revealed that the properties of subhaloes vary according to where they are spatially located within their host halo, with greater difficulties in recovering the input properties of the test subhaloes at small radii (Knebe et al. 2011). Subhalo properties that rely on how their edge is defined, such as their masses, can vary by $\approx 20\%$ between subhalo finders (Knebe et al. 2011; Onions et al. 2012). These differences reflect a combination of how the subhaloes are initially found, and how (and if) the particles are subjected to gravitational unbinding. Overall, phase-space and history-space finders recover the subhalo population properties more robustly than configuration-based finders, although the performance of phase-space finders appears to depend sensitively on their implementation details (e.g. some find similar populations to those in configuration-space finders; Onions et al. 2012).

However, two important aspects are largely missing from past comparisons. First, how the choice of subhalo finder affects cosmologically-relevant summary statistics, e.g. correlation functions. Although discussed in Onions et al. (2012) and Pujol et al. (2014), they focused on either the 10^5 most massive central subhaloes or on the satellites within a relaxed, Milky Way-mass halo. Neither of these choices is a representative subset of the full variety of cosmic structures, so the actual biases may be larger than those inferred from those studies. Second, how the performance of subhalo finders changes between dark-matter-only (DMO) and hydrodynamical simulations. For example, cold and dense gas can be identified as a separate self-bound density peak within a galaxy disc, the phase-space distribution of baryons is clearly different from that in dispersion-supported dark matter haloes, and structure can form non-hierarchically (e.g. tidal dwarf galaxies). Most finders are first developed with DMO in mind, as reflected in previous comparisons of how subhalo finders perform. Hydrodynamical support is subsequently added without consideration of how the effects resulting from the inclusion of baryons affect the algorithms.

Lastly, an equally important aspect is the computational cost of running (sub)halo finding. As simulations grow larger in volume and reach higher resolutions, the speed and scalability of (sub)halo finding becomes an important consideration. Some algorithms are inherently slower than others, leading to a computational expense comparable to the cost of running the simulation itself.

Here, we explore how the choice of subhalo finder affects key summary statistics relevant to large-scale cosmological studies. For this purpose, we use the FLAMINGO simulations (Schaye et al. 2023; Kugel et al. 2023), which constitute a representative suite of simulations for these kind of studies. We focus our comparison on four subhalo finders: HBT-HERONS (a new version of the HBT+ subhalo finder, the previous version of which was described by Han et al. 2018), Subfind (Springel et al. 2005, 2021), VELOCIRAPTOR (Elahi et al. 2019a) and ROCKSTAR (Behroozi et al. 2013a). This set of algorithms is representative of configuration- (Subfind), phase- (VELOCIRAPTOR, ROCKSTAR) and history-space finding (HBT-HERONS).

In this comparison, we find 10% differences in even basic summary statistics like the M_{200c} mass functions. The magnitude of the disagreement between subhalo finders worsens for more detailed properties, like the radial distribution of satellite subhaloes around haloes. Part of the differences is caused by a poorer performance of the algorithms when running in hydrodynamical simulations. Altogether, the aforementioned differences in subhalo finding result in different two-point correlation functions, both in the two- and one-halo regimes. Overall, we find that HBT-HERONS provides a robust and computationally cheap way of identifying subhaloes in simulations. Its history-based approach means that it is able to identify

subhaloes in instantaneous configurations that are difficult to analyse using alternative algorithms. The resulting merger trees contain fewer catastrophic failures (e.g. severe mass swapping and massive transients; Chandro-Gómez et al. 2025), substantially reducing the need to ‘prune’ merger trees in post-processing. Given this, we make the catalogues made by HBT-HERONS the fiducial FLAMINGO ones.

This paper begins by presenting the simulations (§2) and the (sub)halo finders we use (§3). As we present a new version of HBT+, HBT-HERONS, we discuss how it works in more detail than the other subhalo finders. Each change we made to HBT+ is described in detail in Appendix A. The main results of the comparisons across subhalo finders are shown in §4, where we examine the halo & subhalo mass functions (§4.2), the subhalo radial distributions within centrals (§4.3) and the subhalo correlation functions (§4.4). The key takeaway points are summarised in §5.

2 SIMULATIONS

We use the FLAMINGO simulations (Schaye et al. 2023; Kugel et al. 2023) to compare subhalo finders. The FLAMINGO simulations are a suite of large-scale cosmological hydrodynamical simulations calibrated to reproduce the observed $z = 0$ stellar mass function (Driver et al. 2022) and cluster gas fractions (Kugel et al. 2023). The simulations, which also include neutrinos through the δf method (Elbers et al. 2021), were run using the open source code Swift (Schaller et al. 2024) using the SPHENIX SPH scheme (Borrow et al. 2022).

FLAMINGO includes subgrid models for element-by-element radiative cooling and heating (Ploekinger & Schaye 2020), star formation (Schaye & Dalla Vecchia 2008), stellar mass loss (Wiersma et al. 2009; Schaye et al. 2015), feedback energy from supernova (Dalla Vecchia & Schaye 2008; Chaikin et al. 2022, 2023), seeding and growth of black holes, and feedback from active galactic nuclei (Springel et al. 2005; Booth & Schaye 2009; Bahé et al. 2022). AGN feedback is either thermal (Booth & Schaye 2009) or jet-based (Huško et al. 2022). The subgrid parameters were fit to observations using emulators (Kugel et al. 2023), but simulation variations in the feedback strength span the observational uncertainties. In this work, we only analyse the simulations that use the fiducial subgrid model and their dark-matter-only counterparts.

Several FLAMINGO box sizes, resolutions and cosmology variations exist. For this study, we analyse the 1 Gpc³ volumes that use the cosmological parameters from the ‘3x2pt + all external constraints’ dark energy survey year 3 results of Abbott et al. (2022) ($\Omega_m = 0.306$, $\Omega_b = 0.0486$, $\sigma_8 = 0.807$, $H_0 = 68.1$, $n_s = 0.967$). Their initial conditions were generated using a modified version of Monofonic (Hahn et al. 2021; Elbers et al. 2022).

The identifiers of the three resolution levels of the hydrodynamical simulations we analyse, and their corresponding dark matter particle mass (m_{dm}), baryonic particle mass (m_b) and the maximum physical softening length (ϵ) are: L1_m10 ($m_{\text{dm}} = 4.52 \times 10^{10} M_\odot$, $m_b = 8.56 \times 10^9 M_\odot$, $\epsilon_p = 11.40$ kpc), L1_m9 ($m_{\text{dm}} = 5.65 \times 10^9 M_\odot$, $m_b = 1.07 \times 10^9 M_\odot$, $\epsilon_p = 5.70$ kpc) and L1_m8 ($m_{\text{dm}} = 7.06 \times 10^8 M_\odot$, $m_b = 1.34 \times 10^8 M_\odot$, $\epsilon_p = 2.85$ kpc). The particles in the corresponding DMO versions of the simulations have masses: L1_m10_DMO ($m_{\text{dm}} = 5.38 \times 10^{10} M_\odot$), L1_m9_DMO ($m_{\text{dm}} = 6.72 \times 10^9 M_\odot$) and L1_m8_DMO ($m_{\text{dm}} = 8.40 \times 10^8 M_\odot$). From hereon, we omit the _DMO suffix, as we plot the results of hydrodynamical and DMO simulations in separate panels when applicable. The simulations have 79 outputs, with an average spacing in expansion factor of $\langle \Delta \ln a \rangle = 0.015$. The output strategy was not tuned to work with the HBT-HERONS subhalo finder.

3 HALO AND SUBHALO FINDING

In this section, we discuss how we identify (sub)haloes within the simulations. Although the FLAMINGO simulations include neutrinos, we omit them when finding (sub)haloes because they only bind to the most massive structures and they account for a small fraction of the mass ($\Omega_\nu/\Omega_m \approx 4 \times 10^{-3}$). We start by explaining in §3.1 how the Friends-of-Friends (FoF) percolation algorithm works, as it is a required step for each of the subhalo finders we use. We then discuss the working principles behind the four subhalo finders that are compared in this work, which use three distinct approaches: configuration- (Subfind, Springel et al. 2001, 2021), phase- (ROCKSTAR, Behroozi et al. 2013a; VELOCItaptor; Elahi et al. 2019a) or history-space (HBT-HERONS). We conclude this section by discussing how we compute subhalo properties in a consistent manner across finders (§3.6).

Throughout the remainder of the paper, we use the following nomenclature. Haloes are collections of particles found using the 3D FoF particle clustering algorithm, and they contain one or more subhaloes. A subhalo is a self-bound collection of particles distinct from the background in which they are embedded, according to the particular metric that each subhalo finder uses. Subhaloes can be either centrals or satellites, with the position of central subhaloes used as the position of field haloes. The defining property of central subhaloes varies, but they are typically chosen based on comparing a characteristic property (e.g. mass) to other subhaloes within the FoF they are part of (Subfind, VELOCItaptor, HBT-HERONS) or within a given spherical aperture (ROCKSTAR).

3.1 Friends-Of-Friends

All of the subhalo finders we use rely on initially grouping particles using the Friends-of-Friends percolation algorithm. Each distinct FoF group is composed by particles that are within a critical distance from each other, measured using a spatial or phase-space metric. In HBT-HERONS, Subfind and ROCKSTAR, the metric is spatial and set to be a fraction of the mean dark matter interparticle separation. VELOCItaptor also starts with a 3D FoF, but it can subsequently trim it by using a 6D FoF algorithm. This optional step is done with the aim of removing spurious particle bridges, which can boost the halo mass function based on the virial overdensity of Bryan & Norman (1998) (e.g. Euclid Collaboration et al. 2023). In this study, we choose not to use the 6D trimming to find field haloes in VELOCItaptor, as we want to find them as consistently as possible across subhalo finders. This also reflects the same choice as was made for the FLAMINGO halo catalogues presented in Schaye et al. (2023).

The fiducial linking length used by the 3D FoF catalogues in HBT-HERONS, Subfind and VELOCItaptor is set to be 0.2 times the mean interparticle separation. For ROCKSTAR, we use instead the recommended value of 0.28. In the DMO simulations, the mean interparticle separation is defined as:

$$\langle l \rangle_{\text{DMO}} = \left[\frac{m_{\text{dm}}}{(\Omega_{\text{cdm}} + \Omega_b)\rho_{\text{crit}}} \right]^{1/3}, \quad (1)$$

where

$$\rho_{\text{crit}}(z) = \frac{3H^2(z)}{8\pi G}. \quad (2)$$

The baryon density parameter is Ω_b , and the dark matter (minus the contribution of neutrinos) density parameter is Ω_{cdm} . In the hydrodynamical simulations, we use the mean dark matter interparticle separation:

$$\langle l \rangle_{\text{HYDRO}} = \left[\frac{m_{\text{dm}}}{\Omega_{\text{cdm}}\rho_{\text{crit}}} \right]^{1/3}. \quad (3)$$

For HBT-HERONS and Subfind, the linking in hydrodynamical simulations is first done using only the DM particles. All other particle types are subsequently attached to their nearest dark matter-defined FoF group, and those with fewer than 32 total particles are subsequently discarded. In VELOCIRAPTOR, the FoF links pairs of particles as long as one of them is a DM particle. Similar to HBT-HERONS and Subfind, all FoF groups with fewer than 32 total particles are removed from the catalogues. ROCKSTAR runs the FoF algorithm on all particle types directly and by default retains those with more than 10 particles. Each subhalo finder ran its own implementation of FoF, except for HBT-HERONS, which used the FoF output of Swift. We verified that the FoF algorithms implemented within GADGET-4 and Swift produce the same results.

3.2 HBT-HERONS

The HBT-HERONS¹ (**H**ierarchical **B**ound **T**racing - **H**ydro-**E**nabled **R**etrieval of **O**bjects in **N**umerical **S**imulations) algorithm is an updated version of the history-based subhalo finder HBT+ (Han et al. 2018). This new version collects several new additions that improve the identification and tracking of subhaloes in both DMO and hydrodynamical simulations, which are presented in detail in Appendix A². We additionally modified the way in which particles are partitioned within the code to speed it up. This allowed us to run HBT-HERONS using 256 nodes (128 cores per node) on the FLAMINGO-10k DMO simulation (Pizzati et al. 2024; Schaller et al. in prep), which contains over 10080^3 ($\approx 10^{12}$) particles. We also used it to analyse the largest hydrodynamical simulation run to $z = 0$ to date, the 2.8 Gpc FLAMINGO box with 2×5040^3 particles. Given its small computational cost and robust identification of structures, both at fixed and across time (Chandro-Gómez et al. 2025), we make HBT-HERONS our fiducial choice of subhalo finder. In this subsection, we present a general overview of how HBT-HERONS works, with an accompanying diagram to illustrate important steps in Fig. 1.

HBT-HERONS assumes that structure forms hierarchically, i.e. that every present-day subhalo has been a central subhalo in the past. In practice, this means that particles belonging to a given halo become associated to its central subhalo. These memberships are subsequently used to identify the subhalo if it is accreted as a satellite later on. This approach circumvents the difficulties involved when trying to separate heavily overlapping subhaloes. Variations of this history-based approach have recently been used to augment other structure finding algorithms, e.g. Subfind-HBT³ (Springel et al. 2021), MORIA (Diemer et al. 2024) and SYMFIND (Mansfield et al. 2024).

The algorithm requires a series of simulation outputs saved at sufficiently fine time spacing⁴, each containing information on the phase-space distribution and FoF group memberships of particles. Each output is then analysed consecutively, from early to late times. As structures form, they are assigned unique IDs used throughout

the remainder of the simulation. The time-persistence of their IDs facilitates the retrieval of the evolution of the subhalo along its main progenitor branch. The steps each output is subject to are explained below.

3.2.1 Assigning host haloes

The first step consists of assigning a host FoF group to every pre-existing subhalo. Each subhalo has an associated set of N_{tracer} (10 by default) tracer particles, whose type can be constrained to prevent issues when tracking subhaloes in hydrodynamical simulations. For example, allowing gas to be the tracer of a subhalo makes it susceptible to issues arising from gas blowouts (see Appendix A1). By default, HBT-HERONS uses stars and dark matter particles as subhalo tracers, because of their collisionless and time-persistent nature in most cosmological simulations.

The FoF membership of each tracer particle is used to score a list of candidate hosts. Each individual tracer particle is weighted as follows (e.g. Springel et al. 2021):

$$w_i = \frac{1}{1 + \sqrt{r_i}}, \quad (4)$$

where r_i is its bound ranking in the previous output. The sum is done over the $N_{\text{host-finding}}$ (10 by default) most bound particle tracers. The chosen host halo is the FoF group with the highest score out of the candidate list. Once all the pre-existing subhaloes have been assigned to hosts, three distinct possibilities can occur.

First, FoF groups without any assigned subhaloes, and hence no previously existing structures associated to it, are considered potential seeds for new subhaloes. In other words, all of the particles belonging to that FoF group comprise a candidate subhalo. If the candidate subhalo is identified as self-bound, a new central subhalo with a unique ID (TrackID) is created.

Second, the groups that host one or more previously-existing central subhaloes require a decision concerning which subhalo remains as the central (see §3.2.2).

Third, some subhaloes may not be found in any FoF group at all. This occurs primarily near the resolution limit of the simulation, as FoF groups can fragment due to noise and no longer be above the particle number threshold to be found. However, as the particles were previously tagged as being part of a subhalo, HBT-HERONS is able to check if the particles of the now-fragmented FoF remain self-bound. If so, these subhaloes are denoted as hostless, and typically have fewer than 50 bound particles in FLAMINGO.

3.2.2 Identification of the central subhalo

During the assignment of host FoF groups, two or more subhaloes that were centrals in the previous output can be found within the same host halo. This indicates an accretion event has occurred, and a choice about which subhalo is the central needs to be made. Making a sensible choice is important, as it determines which subhalo acquires the particles that have been accreted by its host FoF and that do not already belong to satellites, i.e. diffuse mass accretion (at a given resolution).

To decide which subhalo is the central, all subhaloes in the current FoF group are ranked according to their previous bound mass. The previous bound mass of the most massive subhalo in the previous output, M_0 , is used to define the following threshold:

$$M_{\text{candidate}} = f_{\text{major}} M_0, \quad (5)$$

where $f_{\text{major}} = 0.8$ by default. Only subhaloes whose bound masses

¹ Available at <https://github.com/SWIFTSIM/HBT-HERONS>

² The HBT-HERONS catalogues for FLAMINGO were made without including the centering change described in §A7. The need for that modification only became clear when running on higher resolution simulations.

³ Despite the similarity in the name, the implementation details differ from those in HBT+. This leads to differences that we discuss in Appendix B.

⁴ Han et al. (2012) found that using a time spacing of $\Delta \ln a = 0.2$ leads to a bound subhalo mass function whose amplitude is 5% of the $z = 2.1$ value obtained using a finer time spacing. The convergence improves at lower redshifts and with more frequent outputs. We independently confirmed that FLAMINGO has sufficient outputs to provide "time"-converged mass functions, as there are 79 available outputs with an average spacing of $\langle \Delta \ln a \rangle = 0.015$.

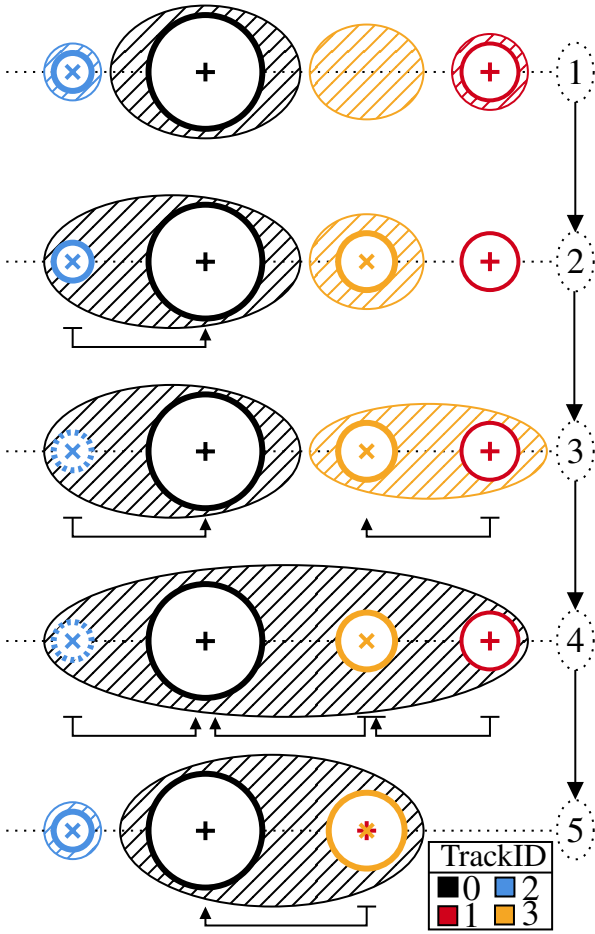


Figure 1. Schematic of how HBT-HERONS tracks subhaloes, shown across five output times. Each column shows the time evolution of a unique subhalo, whose bound component at a given time is represented by a circle. If no bound component is identified, the edge of the circle is dashed. Different colours correspond to different evolutionary branches (‘Tracks’), which have unique IDs (‘TrackIDs’) given by the legend at the bottom. As each TrackID is unique and time-persistent, the evolution of individual subhaloes is easy to retrieve. The shaded ellipses are FoF groups, coloured as their corresponding central subhalo. The lines connecting different subhaloes at a fixed time indicate the current subhalo hierarchy. The crosses and pluses represent the position of its most bound tracer particle. *Output 1:* four FoF groups exist, but one of them does not contain a self-bound subhalo. Only three Tracks (0,1,2) are created. *Output 2:* The FoF without a previous bound subhalo now has one, so a new Track (3) is created. Track 0 and 2 are assigned to the same FoF, based on the weighted FoF membership of their tracer particles. In this case, Track 0 is much more massive than Track 2, so Track 2 is automatically assigned as its satellite. Track 1 is not found in any FoF group, but the past particle membership is used to identify that there is still a bound (hostless) subhalo. *Output 3:* Tracks 1 and 3 are in the same FoF. As they have similar masses, the central subhalo is the one with the minimum kinetic energy in the centre of mass frame of the host FoF (Track 3). Track 2 is now unresolved, so its position and velocity is found using the most bound tracer from output 2. *Output 4:* All subhaloes are found in the same FoF group. Since Tracks 0 and 3 were centrals in the previous output, they are the only candidates to be centrals. Based on the relative mass, Track 0 is chosen as the central, making Track 1 a satellite of a satellite. *Output 5:* The cores of Tracks 1 and 3 overlap in phase-space, so they are merged into a single subhalo. The tracer of Track 2 is found in a separate FoF, i.e. it is a splashback object. The FoF hosting Track 2 has no resolved subhaloes at that time, meaning that its particles are assigned to the orphaned Track 2. The particles are then confirmed to be self-bound, making Track 2 appear as a resolved subhalo again.

in the previous output were above this threshold are considered central candidates. Thus, the choice is trivial if only minor accretions occur.

If more than one subhalo satisfies the above mass threshold, the specific orbital kinetic energy of each candidate is computed in the centre of mass reference frame of the host FoF group. The subhalo candidate with the lowest value, and hence moving most like its host FoF group, is chosen as central. Updating which subhaloes are assigned to be satellites also propagates to the hierarchy of structures that they brought with them, e.g. their satellites become satellites of satellites.

3.2.3 Mass accretion

The evolution of central and satellite subhaloes is manifestly different. Centrals generally grow in mass, whereas the growth of satellites typically halts or becomes negative after being accreted. HBT-HERONS therefore only allows the centrals of each FoF group to accrete new mass in diffuse form. Satellites can still accrete mass, but only if the mass has been stripped from one of their own satellites. Conversely, although for centrals the acquisition of particles is generally limited to those which are not already associated to resolved satellites, mass can still be accreted from satellites if the particles are not bound to them, as explained in §3.2.4.

An important aspect of the tracking of which particles belong to which subhalo is the notion of the ‘source’ subhalo (see Han et al. 2012). This is the initial set of particles passed to the unbinding routine when checking for its self-boundness. The way in which it is defined differs across subhalo finders, and is closely related to the performance with which they identify subhaloes. Taking `Subfind` as an example, the source subhalo corresponds to all particles enclosed within a density peak in configuration space, excluding additional density peaks within. HBT-HERONS defines it based on the past evolution of subhaloes.

For the simplest case of a single (central) subhalo in a FoF group, all of the particles in the FoF group are initially part of its source, modulo the truncation that occurs after unbinding (see §3.2.4). The source particles belonging to said subhalo are tracked forward in time, so that if it is subsequently found as a satellite, they are used to separate it from the background particles belonging to the more massive subhalo. In this configuration, the central has as its source all the particles that are part of the FoF, except for those that already belong to the sources of resolved satellite subhaloes.

3.2.4 Unbinding

The hierarchy of structures within each FoF group is analysed recursively from the bottom of the subhalo hierarchy. In other words, the subhaloes without any children are subject to unbinding first, at which point their parents can be analysed. The process is repeated until the central subhalo of the FoF is analysed. This depth-first approach allows for the possibility of parents gaining bound mass that is not bound to its children subhaloes.

The unbinding of a single subhalo is done iteratively, whereby its centre of mass velocity and position is updated based on the particles deemed to be bound in any given iteration. To speed up the process of unbinding, the particle distribution is subsampled if the subhalo contains more than $N_{\text{subsample}}$ (1000 by default) particles. In practice, this can lead to small differences in the subhalo bound mass functions at the high mass end between different runs of HBT-HERONS on the same simulation. This reflects different random numbers being generated when doing the particle subsampling.

Additionally, the threshold used to determine whether the iterative unbinding has converged can be changed to reduce the number of iterations. The threshold used to stop the iterations is defined based on the ratio of bound particles (N_{bound}) between two consecutive iterations: $N_{\text{bound}}^{i+1}/N_{\text{bound}}^i \geq f_{\text{converge}}$, where $f_{\text{converge}} = 0.995$ by default.

As mentioned previously, each satellite subhalo has its own source subhalo. Despite the possibility of accreting mass from its own children subhaloes, more bound mass is typically lost than gained. Therefore, the source component is generally larger than the set of bound particles. Although tracking the particles in this manner is crucial to separate satellite subhaloes from the background of their host, without adequate care it can lead to failures in subhalo finding. For example, if the source subhalo is dominated by particles that are truly unbound, the centre of mass estimate can be offset from the true centre of the subhalo. Consequently, the kinetic energies in its core will be biased high, as the Hubble flow contribution (proportional to the distance to the centre of mass) is larger. This can lead to an apparently unbound core, even though it is purely driven by an incorrect choice of reference frame.

To prevent such instabilities during unbinding, HBT-HERONS limits the number of particles that any source subhalo can have ($N_{\text{source}}^{\text{max}}$). By default, it equals three times the number of bound particles, i.e. $N_{\text{source}}^{\text{max}} = 3N_{\text{bound}}$. After the unbinding step, the least bound particles of the source subhalo are removed until $N_{\text{source}} \leq N_{\text{source}}^{\text{max}}$. If possible, the particles removed from the source subhalo are accreted by the source of its parent subhalo.

Lastly, if a previously resolved subhalo no longer has enough bound particles to be above the threshold to be classified as self-bound ($N_{\text{bound}}^{\text{min}}$; 20 by default) or has insufficient tracer particle types ($N_{\text{tracer}}^{\text{min}}$; 10 by default), it becomes an orphan. The position and velocity of orphan subhaloes, which are often used in the context of semi-analytical models of galaxy formation (e.g. [Kitzbichler & White 2008](#); [Guo & White 2014](#)), are subsequently tracked by their most bound tracer particle when the subhalo was last resolved. Note that if the tracer particle is found in a FoF host without currently resolved subhaloes, the particles are acquired by the source of the orphan subhalo. This means that if they are found to be bound, orphans can re-appear in the simulation.

3.2.5 Merging

Pairs of structures with similar masses can merge as a consequence of dynamical friction, whereby the lower mass one loses orbital energy and eventually becomes deeply embedded in the core of its host. This process is sometimes insufficient to disrupt the sinking subhalo ⁵, which for a tracking subhalo finder like HBT-HERONS can result in persisting subhaloes that heavily overlap in phase-space. This is not a problem for other methods of halo finding, since density peaks would coalesce into one and configuration and phase-space finders would in principle not find two separate subhaloes.

To prevent this unwanted behaviour, which would lead to artificially high numbers of objects in the central regions of subhaloes, HBT-HERONS merges subhaloes that are within a threshold phase-space offset. This offset is defined for two pairs of subhaloes within

⁵ If the sinking process does not sufficiently disturb the subhalo so as to disrupt it, checking its self-boundness is similar to checking the self-boundness of a subset of the most bound particles of its host halo. Hence, it is likely to be found as self-bound.

the same hierarchical tree branch, i, j , as:

$$\Delta = \frac{|\vec{x}_i - \vec{x}_j|}{\sigma_{i,x}} + \frac{|\vec{v}_i - \vec{v}_j|}{\sigma_{i,v}} \quad (6)$$

Here, σ_x and σ_v are, respectively, the position and velocity dispersion of the 10 most bound tracer particles of the parent subhalo, which are also used to compute its position \vec{x}_i and velocity \vec{v}_i . The position and velocity of the subhalo located deeper in the hierarchy ⁶ are also estimated using its 10 most bound tracer particles.

This condition is checked between pairs of subhaloes contained in the same hierarchical tree branch, e.g. TrackIDs 0, 3 and 1 in output 4 of Fig. 1. If $\Delta \leq 2$, the less massive subhalo is marked as merged, and all of the particles in its source subhalo are acquired by the more massive one. This is followed by a new unbinding of the subhalo that accreted the mass, to update its bound mass based on the gravitational potential that includes the newly accreted mass.

As merger checks can only happen between subhaloes that share an explicit hierarchical connection, not all potential satellite-satellite merger configurations are handled by HBT-HERONS. For example, the current approach is unable to account for mergers between satellite subhaloes that were independently accreted as separate centrals, but subsequently encounter each other at sufficiently low velocities so as to form a bound system. The fact that the subhaloes were accreted separately means that no hierarchical relation links them, and hence no merger checks occur between them. Future work will modify HBT-HERONS to be able to handle such encounters.

3.3 Subfind

In this work, we use the Subfind version that is available within the public version of GADGET-4 ([Springel et al. 2021](#)). To identify subhalo candidates within a FoF group, its member particles are used to estimate the local total mass density field via adaptive kernel estimation. The resulting density peaks are seeds for potential subhaloes, which grow through an excursion set algorithm until they reach saddle points that connect them to neighbouring peaks.

The self-boundness of each candidate subhalo is checked by an iterative unbinding process. All particles are considered initially, with subsequent iterations only using those deemed as bound for gravitational potential calculations. In each step, the centre of mass reference frame of bound particles is used, and only a fraction of particles can be removed at a time. Iterations stop whenever the subhalo is deemed as disrupted (20 particles by default), or the number of bound particles has converged ($N_{\text{bound}}^{i+1}/N_{\text{bound}}^i = 1$).

3.4 ROCKSTAR

The position and velocity dispersion of particles (σ_x, σ_v) associated to the initial 3D FoF group defines a length and velocity scale used to define a phase-space distance between two particles i, j :

$$d(\vec{x}_i, \vec{v}_i; \vec{x}_j, \vec{v}_j) = \sqrt{\frac{|\vec{x}_i - \vec{x}_j|^2}{\sigma_x^2} + \frac{|\vec{v}_i - \vec{v}_j|^2}{\sigma_v^2}}. \quad (7)$$

Particles are linked if they are within a certain phase-space distance. The threshold value is found by requiring that a minimum specified fraction of particles (0.7 by default) have at least one

⁶ In HBT-HERONS, depth refers to the number of hierarchical connections that a given subhalo is away from the central subhalo of its host FoF group. A central subhalo thus has a depth of 0, its satellites a depth of 1, the satellites of satellites a depth of 2, etc.

neighbour. This process is repeated for each subsequent 6D FoF group that has more than a predefined number of associated particles (10 by default), to find substructures within substructures. Particles in the 3D FoF are assigned to the closest seed subhalo in phase-space based on a distance metric similar to equation (7), where the position normalisation σ_x is replaced by a characteristic radius $r_0 \equiv V_{\max} t_{\text{vir}} = V_{\max} (4\pi G \rho_{\text{vir}}/3)^{-1/2}$. Here, ρ_{vir} is the virial density as defined in Bryan & Norman (1998).

Contrary to the other subhalo finders used in this work, ROCKSTAR only does a single unbinding iteration, and keeps all subhaloes whose 6D FoF group contains more than a specified fraction of bound particles (0.5 by default). This approach is computationally cheap, although an iterative unbinding approach is able to cut down the number of spurious subhaloes and identify otherwise unresolved ones, as discussed in Griffen et al. (2016). In this work, we use the default of a single unbinding pass, to reflect the choice made in other large-scale cosmological simulations, such as the Euclid flagship simulations (Euclid Collaboration et al. 2024b). Another difference relative to the other three subhalo finders is that ROCKSTAR includes particles that belong to parent subhaloes in the calculation of particle gravitational potentials if the subhalo being analysed is undergoing a major merger. The most important difference for the purposes of this study is that ROCKSTAR allows particles to be bound to multiple subhaloes at once (i.e. it uses an *inclusive* mass assignment), whereas the other three subhalo finders only allow any given particle to be bound to one subhalo (i.e. *exclusive* mass assignment). We outline how we address this difference in §3.6.

Another choice concerns how to run ROCKSTAR on hydrodynamical simulations. Some studies do the 6D FoF linking using all particle types, which is the default behaviour of `rockstar-galaxies` (e.g. Hahn et al. 2017; Villaescusa-Navarro et al. 2023). Others restrict the FoF linking to be done on dark matter particles first, and subsequently rely on a post-processing step to assign stellar masses to each subhalo (e.g. Necib et al. 2019; Jung et al. 2024). In the main analysis of study, we use all particle types except black holes⁷ during linking and unbinding, as per the recommended way of using `rockstar-galaxies` (Behroozi; private communication). The alternative would neglect the contribution of baryons to the gravitational potential, which could lead to identifying baryon-dominated objects as less massive or even disrupted. Nonetheless, we provide a brief comparison in Appendix D of how basic summary statistics change between these two analysis choices.

3.5 VELOCraptor

VELOCraptor uses a different approach to identify structure in phase-space compared to ROCKSTAR. The core idea behind its subhalo finding implementation is that the centres of subhaloes are not only peaks in the density field, but also have colder velocity distributions than the surrounding background particles. This means their cores appear as peaks in both the spatial and velocity density fields.

To identify the velocity peaks, VELOCraptor first estimates the expected *background* velocity density distribution for each particle, f_{bg} . For this purpose, it assumes that the background velocity density follows a multivariate Gaussian distribution (e.g. Vogelsberger et al.

2009):

$$f_{\text{bg}} = \frac{\exp\left[-\frac{1}{2}\Delta\vec{v}\langle\Sigma_v\rangle^{-1}\Delta\vec{v}\right]}{(2\pi)^{3/2}|\langle\Sigma_v\rangle|^{1/2}}. \quad (8)$$

Here, $\langle\Sigma_v\rangle$ is the mean local velocity dispersion tensor, and $\Delta\vec{v}$ is the velocity of the particle relative to the mean background velocity, $\vec{v}_i - \langle\vec{v}\rangle$. Both $\langle\vec{v}\rangle$ and $\langle\Sigma_v\rangle$ are computed using a mass-weighted average of all particles within a rectangular cuboid built using a kD-tree algorithm. The values between adjacent cells are subsequently interpolated onto the positions of individual particles using inverse distance weighting.

The *local* velocity density of an individual particle, f_i , is computed using Epanechnikov kernel smoothing (Sharma & Steinmetz 2006) with its closest neighbouring particles in velocity, themselves chosen from its closest spatially neighbouring particles. The ratio between local and background velocity densities, $\mathcal{R} = \ln f_i/f_{\text{bg}}$, is proportional to the likelihood that the particle is associated to a dense and cold structure, e.g. a subhalo. The actual likelihood is computed as:

$$\mathcal{L}_i \equiv \frac{\mathcal{R}_i - \langle\mathcal{R}\rangle}{\sigma_{\mathcal{R}}}, \quad (9)$$

where $\langle\mathcal{R}\rangle$ and $\sigma_{\mathcal{R}}$ are the mean and standard deviation of a skewed Gaussian fitted to the binned distribution of \mathcal{R} .

Particles are then grouped by first applying a cut on the minimum required value of \mathcal{L}_i , by default 2.5, and then linking them in phase space using a FoF-like algorithm. The spatial linking is done in a similar way as the 3D FoF algorithm, but the linking length is halved and hence targets higher overdensities. The linking in velocity space is based on the velocity ratio between particles and the angle between velocity vectors. Finally, all candidate subhaloes are subject to unbinding. If the number of particles within a subhalo is sufficiently high, this whole process is iteratively repeated on its particle members until the resulting subhaloes have fewer than a threshold number of particles (800 by default).

3.6 Halo and subhalo properties

Different subhalo finders calculate (sub)halo properties under different sets of assumptions and choices. For example, spherical overdensities are computed using only bound particles in ROCKSTAR and HBT-HERONS, whereas `Subfind` and `VELOCraptor` include all particles regardless of subhalo membership. Moreover ROCKSTAR assigns mass in an *inclusive* manner, whereas all the other subhalo finders used in this work assign mass *exclusively*. This drives differences in population statistics purely due to operational definitions, rather than the performance of each (sub)halo finder. Therefore, in order to compare different structure finding algorithms, the definition of mass and the computation of properties need to be as consistent as possible.

To do so, we modified ROCKSTAR so that it assigns masses to subhaloes exclusively, similar to what is done in the other subhalo finders we compare in this work. We also compute properties for HBT-HERONS, `Subfind` and `VELOCraptor` subhaloes using SOAP⁸ (Spherical Overdensity and Aperture Processor; McGibbon et al. in prep.). SOAP is a Python package that computes a variety of subhalo properties in different spherical and projected apertures, both with and without taking into account the bound membership of particles.

⁷ The inclusion of black holes resulted in structures that spanned over 10 Mpc in length, which no longer happened once we removed them from the FoF linking.

⁸ Available at <https://github.com/SWIFTSIM/SOAP>

In short, SOAP loads the centres of subhaloes and memberships of particles as given by each subhalo finder⁹, and computes the properties of interest using the same routines, hence circumventing additional choices made by each particular halo finding algorithm. We explore how the changes we made to the mass assignment in ROCKSTAR and how SOAP-computed M_{200c} values differ from those provided by subhalo finders in Appendix E.

In this study, we calculate three different subhalo properties: their bound mass (M_{bound}), the maximum circular velocity (V_{max}) and the virial mass (M_{200c}) if the subhalo is a central. The last two properties require passing a subhalo centre to SOAP, as they use spherical apertures to compute their values. The definition of a subhalo centre differs among codes. HBT-HERONS uses the position of the most bound particle. Subfind and VELOCIRaptor use the position of the particle with the largest value of the gravitational potential energy. Lastly, ROCKSTAR uses the centre of mass position of the particles that are bound to the subhalo.

The bound mass is simply the sum of the mass of all particles bound to a subhalo. We note that we include the thermal energy of gas when subjecting subhaloes to unbinding across every subhalo finder. The value of V_{max} corresponds to the peak value of the circular velocity rotation curve, which is defined as:

$$V_{\text{circ}}(r) = \sqrt{\frac{GM(<r)}{r}}. \quad (10)$$

Here, only particles that are bound to the subhalo contribute to the sum at a given radius. We also apply the constraint that no particles can be less than a gravitational softening length (ϵ) away from the centre of the subhalo. In other words, we constrain $R_{\text{max}} \geq \epsilon$. This removes unrealistically high values of V_{max} driven by particle sampling noise in the inner core of subhaloes.

We define the value of M_{200c} by summing up the total mass within a spherical region whose mean density is 200 times the critical density of the Universe, i.e.

$$M_{200c} = \frac{4\pi R_{200c}^3}{3} \times 200\rho_{\text{crit}}. \quad (11)$$

The value is found by iteratively increasing the radius of a sphere placed on the subhalo centre until the mean density is less than $200\rho_{\text{crit}}$. The value of R_{200c} is interpolated between the particles adjacent to where the drop below $200\rho_{\text{crit}}$ occurs, to obtain the exact target overdensity. Note that we only compute M_{200c} for central subhaloes, and include the mass contribution of all particles within the aperture, regardless of whether the enclosed particles are bound to the central or not. This means that, despite not using neutrinos when identifying (sub)haloes, we account for their mass contribution enclosed within the R_{200c} of each halo.

4 RESULTS

We start this section by illustrating how the choice of subhalo finder affects the structures found in the vicinity of a cluster-mass halo, in its DMO and hydrodynamical versions (§4.1). We then proceed to discuss how the differences propagate to three summary statistics commonly used in cosmology: halo and subhalo mass functions

⁹ ROCKSTAR does not provide the bound membership of particles in its outputs, meaning that we only use SOAP for the values of M_{200c} . However, bound memberships are only required for bound mass and maximum circular velocity calculations. We have verified that the relevant routines in SOAP and ROCKSTAR are identical.

(§4.2), radial distributions of subhaloes around haloes (§4.3) and the correlation functions of subhaloes based on a V_{max} selection (§4.4).

Before discussing the results, we note how long it took to run each subhalo finder on the $z = 0$ snapshot of the DMO L1_m9 box. In our tests, the slowest were Subfind and VELOCIRaptor, which took $O(1000)$ CPU-h to run. The fastest were HBT-HERONS¹⁰ and ROCKSTAR, taking only $O(10)$ CPU-h to run. For HBT-HERONS, Subfind and VELOCIRaptor the times taken to run on the hydrodynamical versions are about two to three times slower than for the corresponding DMO analysis. ROCKSTAR actually took less time to run on the hydrodynamical simulation, likely due to the problems it suffers from when trying to find subhaloes when linking all particle types, as discussed below.

4.1 Representative example

We select a dark matter halo of $M_{200c} = 2.3 \times 10^{15} M_{\odot}$ from the L1_m9 box ($m_{\text{dm}} = 5.65 \times 10^9 M_{\odot}$ in the hydrodynamical version) that is undergoing a three-way merger at $z = 0$. The projected density of dark matter within a thin slice of its central region is shown in Fig. 2. Its clearly identifiable merging companions provide a good test-bench for how well the subhalo finders are able to decompose heavily overlapping subhaloes. Note that this test makes the implicit assumption that every visible density peak is caused by the presence of a subhalo.

The positions of all subhaloes with at least 20 bound particles are highlighted using circles. Their colours encode whether the subhaloes are centrals (magenta) or satellites (blue dashed). Focusing on the image from the DMO simulation, it is clear that differences in the satellite population exist across different subhalo finders. VELOCIRaptor and Subfind do not find the subhalo associated to the second most prominent density peak, which is located just below the central subhalo. Additionally, VELOCIRaptor also misses a companion subhalo just below it. ROCKSTAR finds the two subhaloes that VELOCIRaptor and Subfind miss, but fails to find two subhaloes in the lower left quadrant that are found by all other subhalo finders. HBT-HERONS is the only finder capable of identifying all of the visually detectable subhaloes in the central regions of this example.

Several subhaloes without visual counterparts are found in the outskirts of the image of the DMO version. These subhaloes are near the resolution limit of the simulation, but their existence and location is generally found to be consistent across subhalo finders. The outlier is ROCKSTAR, which finds four additional subhaloes in the upper left quadrant that are not found by the other finders. Additionally, the subhalo it finds in the right hand side of the imaged region is clearly offset from the location that other finders identify. ROCKSTAR also finds a centre for the central companion that is evidently offset from its associated density peak.

Turning to the hydrodynamical counterpart of the same halo, we see that the number of resolved subhaloes increases for all subhalo finders. The associated density peaks in the projected DM surface density maps are more prominent, suggesting that the central dark

¹⁰ The time for HBT-HERONS is for a single time output, but it needs to analyse all preceding ones. Nonetheless, its speed-up relative to the slowest subhalo finders means that it is sometimes cheaper to process all outputs with HBT-HERONS instead of just one with another subhalo finder. Additionally, if one is interested in the time evolution of subhaloes, all of the other subhalo finders would need to be run on all outputs too, as well as running a merger tree algorithm.

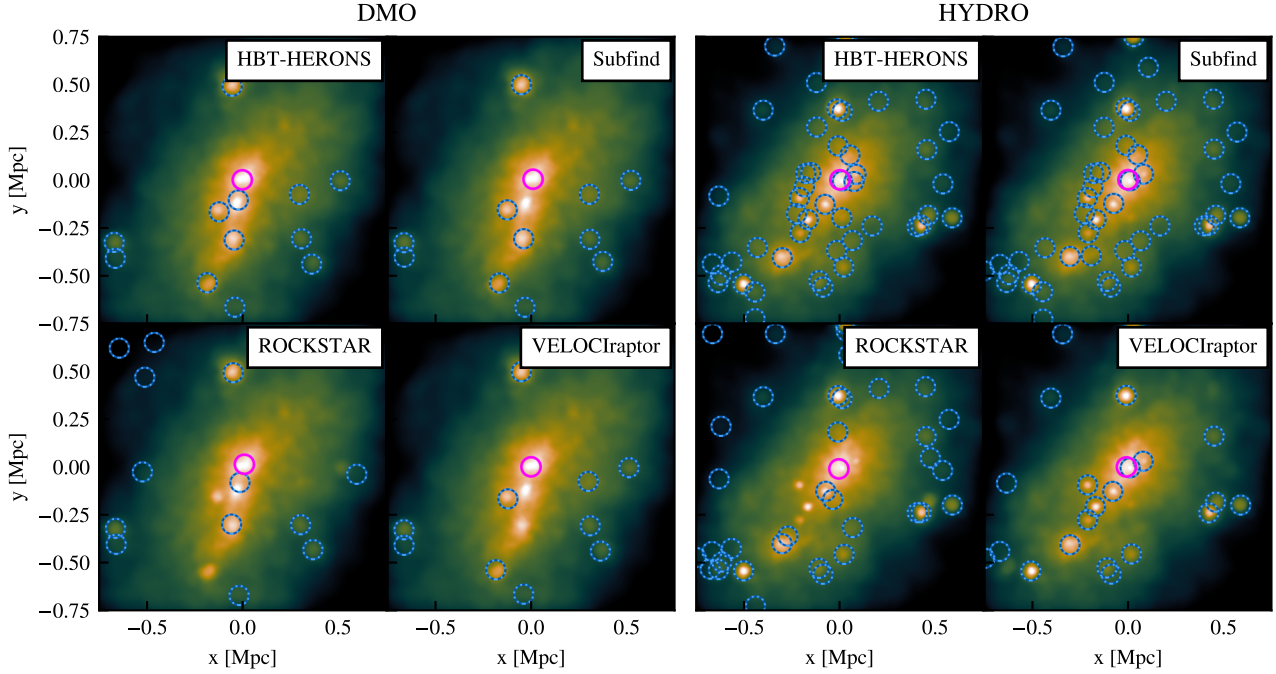


Figure 2. Projection of the dark matter density along a volume of side-length 1.5 Mpc and depth 0.4 Mpc. The centre was chosen to be the HBT-HERONS-identified centre of a $M_{200c} = 2.3 \times 10^{15} M_{\odot}$ halo, the second most massive of the L1_m9 DMO simulation. Its counterpart in the hydrodynamical version of the box is shown in the right set of images. The colour map scale is consistent across all panels. The circles indicate the location of resolved subhaloes found by each subhalo finder, as indicated in the top right corner of each image. The colour of each circle indicates whether they are centrals (magenta) or satellites (blue dashed).

matter distribution has contracted and become denser in response to the presence of galaxies at their centres. Differences remain between subhalo finders, with HBT-HERONS and Subfind finding the most subhaloes. There is a distinct lack of VELOCIRaptor subhaloes in the outskirts, most of which are poorly sampled. ROCKSTAR misses clearly identifiable subhaloes in the central regions, though we note that catalogue is likely influenced by our choice to run its 6D FoF group finding on all particle types. ROCKSTAR provides the most extreme example of how the performance of subhalo finders can change between DMO and hydrodynamical simulations.

4.2 Mass functions

The (sub)halo mass function measures the number density of dark matter (sub)haloes as a function of a given mass definition. For many applications, the mass enclosed within a given spherical overdensity is used for central subhaloes. Alternative definitions rely on the mass that is self-bound, and are particularly useful when dealing with satellite subhaloes, which are embedded within a more massive central subhalo.

In this subsection, we explore how sensitive alternative definitions of masses are to the choice of (sub)halo finder. Since V_{\max} is another commonly used metric to quantify the mass of subhaloes, we also include it in this analysis. Given that we are interested in the differences across finders, we always express the measured mass functions relative to what is found using HBT-HERONS. We also discuss the convergence of these quantities across resolution levels when relevant.

4.2.1 Halo mass functions

We show the $z = 0$ M_{200c} mass functions across subhalo finders and expressed relative to HBT-HERONS in Fig. 3. The M_{200c} is computed by SOAP, and it corresponds to the total mass enclosed within a spherical region that is 200 times denser than the critical density of the Universe. The only inputs required from each subhalo finder are which subhaloes are centrals, and where their centres are located. Therefore, one might expect this statistic to be less sensitive to the choice of subhalo finder, compared to those based on mass that rely on identifying which particles are bound to a given subhalo.

Focusing first on the DMO simulation in the top panel of Fig. 3, we see good agreement between HBT-HERONS and Subfind irrespective of the resolution of the simulation. The median difference is much less than 1% across the mass range we consider here. As both subhalo finders rely on the same spatial 3D FoF group catalogue, the similarities between their mass functions suggest that the centre locations of the centrals are, on average, similar. However, we note that there are still some differences in the location of individual haloes between HBT-HERONS and Subfind, simply due to the choice of which subhalo within a FoF group is the central (see Appendix C). Despite this, the differences are not systematic, and are averaged out when measuring the M_{200c} mass function of the whole population of haloes.

Larger differences appear when comparing to VELOCIRaptor. The mass function is systematically suppressed at the high-mass end by up to 3% regardless of the resolution of the simulation. The difference relative to HBT-HERONS becomes progressively smaller at lower masses, and it is within 1% below $M_{200c} \approx 8 \times 10^{13} M_{\odot}$. The aforementioned suppression at large masses is somewhat surprising,

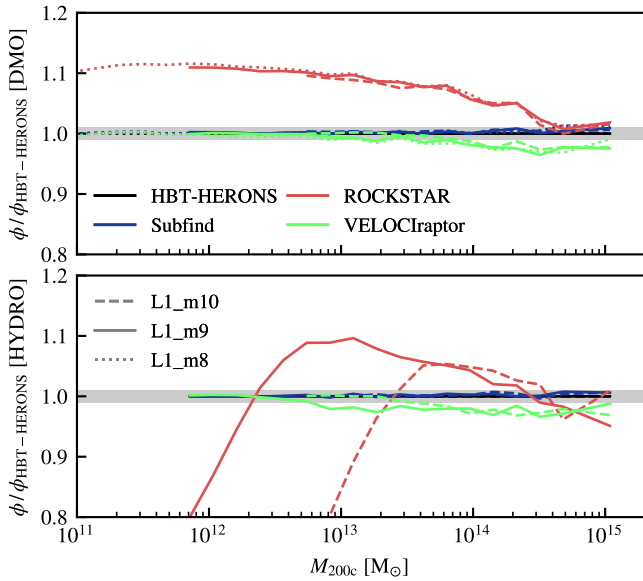


Figure 3. Number density of central subhaloes as a function of their associated M_{200c} mass. The top panel is for the DMO version of the box, and the bottom panel for the HYDRO version. Each coloured line indicates the mass function found using a different subhalo finder, which are expressed relative to the one found using HBT-HERONS at the same resolution. Different resolutions are indicated by the styles of the lines. Only the mass range corresponding to masses greater than the equivalent of 100 DMO dark matter particles (at a given resolution) is shown. The shaded region highlights differences smaller than 1%.

as VELOCIRaptor assigns a single central subhalo per individual FoF group, similar to what HBT-HERONS and Subfind do. As the FoF groups for these three finders are all built using a spatial FoF with a linking length of 0.2 times the mean interparticle separation, the difference likely stems from where the centres of the spherical overdensity apertures are placed.

We investigate the discrepancy with VELOCIRaptor in more detail in Appendix C. In short, we bijectively match central subhaloes between subhalo finders, and measure the spatial offset and M_{200c} ratio relative to the values found in HBT-HERONS. We find that a fraction of high-mass central subhaloes are miscentred in VELOCIRaptor. In such cases, the centre is incorrectly identified with the location of a satellite, leading to lower values of M_{200c} relative to all the other subhalo finders (Fig. C1). Some examples have an M_{200c} whose value is lowered by an order of magnitude.

Despite the miscentering of VELOCIRaptor, the most discrepant mass function is the one found using ROCKSTAR. It is within 1% of the value found by HBT-HERONS above $M_{200c} \approx 4 \times 10^{14} M_{\odot}$, but the differences quickly exacerbate towards lower masses. This results in a disagreement in the halo mass functions at the 10%-level relative to all other subhalo finders considered in this work. Contrary to VELOCIRaptor, the differences are not due to the positioning of central subhaloes (see Appendix C). The cause is the definition of central subhaloes, which differs from the other subhalo finders, as was also discussed in Euclid Collaboration et al. (2023).

HBT-HERONS, Subfind and VELOCIRaptor assign a single central subhalo per FoF group. This is done by identifying the most massive one (HBT-HERONS & Subfind) or the one found before doing refined searches in velocity space (VELOCIRaptor). ROCKSTAR does not use FoF information to decide which subhaloes are centrals. Instead, it relies on building a hierarchy of subhalo parent-children connections based on their spatial distribution and measured properties. Starting

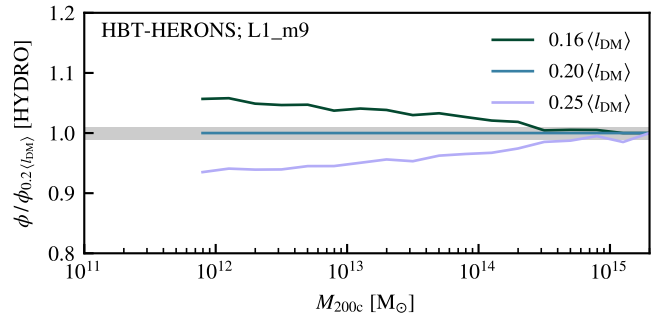


Figure 4. Similar to Fig. 3, but showing how the M_{200c} mass function changes for the hydrodynamical version of the L1_m9 simulation when using different FoF linking lengths. The results obtained using shorter and longer linking lengths, which target higher and lower overdensities respectively, are expressed relative to the fiducial value of $0.2 \langle I_{DM} \rangle$.

from the subhalo with the highest V_{\max} in the simulation, it searches for all subhaloes within its virial radius (R_{vir}). The virial radius is computed for all subhaloes, using only the particles bound to them and based on the spherical overdensity of Bryan & Norman (1998). All neighbouring subhaloes whose R_{vir} and V_{\max} values are smaller are assigned as its children. This process is repeated for all subhaloes in a decreasing V_{\max} order, and the subhaloes which have no parents at the end of this process are deemed centrals.

In practice, this choice of central definition leads to many subhaloes that are identified as satellites in the other subhalo finders being classified as centrals in ROCKSTAR. This in turn leads to more spherical overdensities being computed, and hence boosts the number density of subhaloes at fixed M_{200c} . Of course, one may argue about which central definition is the more appropriate one. On the one hand, FoF-based central identification can be sensitive to spurious particle bridges. On the other hand, physical overdensities do not distinguish between bound and unbound material, and should arguably only be defined for virialised subhaloes that have not been stripped. However, bound-only variants are required to assign ‘virial’ radii to satellite subhalos, as not excluding unbound particles may lead to their ‘virial’ radii being much larger than their actual physical extent. In practice, the approach that ROCKSTAR uses means that the assignment of virial radii becomes strongly dependent on the bound mass of a given subhalo, and hence how its particles are subject to unbinding.

Leaving aside the discussion of which definition of central is more appropriate, which in any case will depend on the application, the differences we see highlight the current freedom in choosing the definition of what constitutes a central. As we show here, this propagates directly to predicted summary statistics, and will bias inferences based on comparisons to observations.

We show the M_{200c} mass functions measured from the hydrodynamical simulations in the bottom panel of Fig. 3. We only computed them for the L1_m10 and L1_m9 versions due to the increasingly high computational cost of running Subfind. The overall trends are similar to those we found for the DMO simulation. However, the suppression of the halo mass function of VELOCIRaptor now extends to even lower masses ($\approx 5 \times 10^{12} M_{\odot}$). This happens because the miscentering worsens when baryons are included. In essence, it results from more satellites missing from the VELOCIRaptor catalogues, which means that the satellite particles are assigned to be part of the central subhalo instead. The relatively dense distribution of particles that are located around the centres of missing satellites are conducive to having the centre of the field halo being placed there.

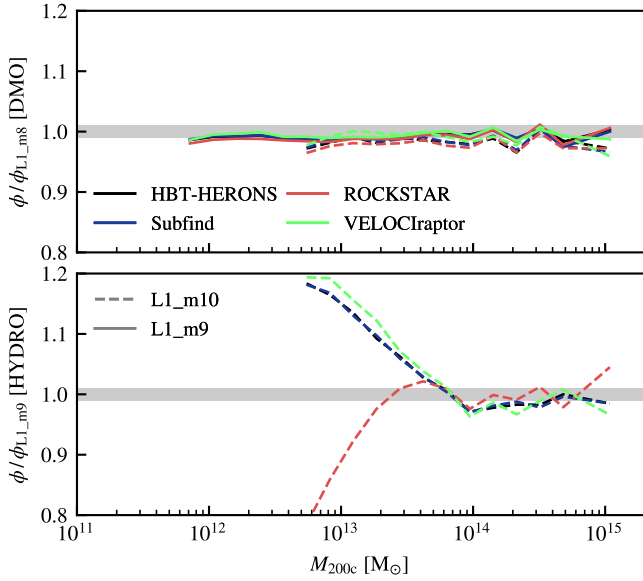


Figure 5. Similar to Fig. 3, but showing how the M_{200c} mass function converges across resolution levels using different subhalo finders. The mass functions for a given subhalo finder are normalised to the mass function obtained from the same subhalo finder using the highest resolution simulation available for that box (L1_m8 for DMO and L1_m9 for hydro).

The ROCKSTAR mass function in the hydrodynamical simulation now has a suppression in the number density of both low- and high-mass haloes relative to HBT-HERONS. As discussed in §4.1, this is likely caused by the issues that arise in halo finding when using all particle types for 6D FoF finding. To explore whether this behaviour remains when excluding baryons from the FoF calculations, we ran it using only DM particles. As shown in Appendix D, in that case the M_{200c} functions show a similar behaviour to what was found in the DMO version, indicating that the linking of different particle types is the culprit of the differences.

Returning to the way in which centrals are defined, beyond the details of how to assign radii to subhaloes, the way in which spherical exclusivity is defined can affect the resulting mass functions by up to 6% within ROCKSTAR (García & Rozo 2019). Presumably, the measured M_{200c} mass function using subhalo finders that assign one central per FoF group can also be influenced by the choice of linking length used within the FoF algorithm. Changing the linking length will change the number of FoF groups, and hence the number of central subhaloes within the same simulation box. The need to choose a linking length constitutes an uncertainty in comparisons with observations, given that observed objects are obviously not identified using a FoF algorithm run on dark matter particles.

As the fiducial FoF linking length of 0.2 times the mean dark matter interparticle separation is not obviously the best a priori choice when comparing against observations, we test the effect of different linking lengths on the M_{200c} mass function. We do this by changing its value to be 0.16 and 0.25 of the mean dark matter interparticle separation $\langle l_{DM} \rangle$. These values roughly correspond to a change of a factor of 2 in overdensity relative to the fiducial linking length of $0.2\langle l_{DM} \rangle$. After constructing these new FoF catalogues for the hydrodynamical version of the L1_m9 simulation, we run HBT-HERONS to identify the $z = 0$ central subhaloes and measure their M_{200c} masses using SOAP.

The resulting mass functions are shown in Fig. 4. We see a clear mass-dependence on the measured mass function relative to the fiducial FoF linking choice. The shorter linking length ($0.16\langle l_{DM} \rangle$),

which targets higher overdensities, results in a steeper mass function than the fiducial linking length ($0.2\langle l_{DM} \rangle$). This in turn yields an increase of 5.8% in the number density of $\approx 10^{12} M_{\odot}$ haloes, which is not as large of a difference compared to that caused by the central definition used in ROCKSTAR. Conversely, the longer linking length of $0.25\langle l_{DM} \rangle$ that selects lower overdensities, results in shallower mass functions. The abundance of $\approx 10^{12} M_{\odot}$ haloes is instead lowered by 6.5% relative to the fiducial linking length. The differences decrease with increasing halo mass, but only become smaller than 1 per cent for $M_{200c} \geq 5 \times 10^{14} M_{\odot}$. We note that, although this test was only done using HBT-HERONS, we expect our findings to be applicable to any subhalo finders that assign a single central subgroup per 3D FoF group. In this study, this applies to Subfind and VELOCraptor.

Another important aspect when considering the effect of subhalo finders on the measured M_{200c} mass functions is how well they converge across resolution levels. In principle, there is no guarantee that different subhalo finders converge to the result they find at the high resolution simulation at the same rate. In other words, one algorithm may perform particularly poorly in high resolution simulations relative to lower resolution counterparts, or vice versa. Thus, we conclude this subsection by exploring the convergence of the M_{200c} mass functions for different subhalo finders in Fig. 5. For this purpose, we normalise the mass functions found by each subhalo finder using the mass function that the same subhalo finder obtained for the highest resolution simulation with available catalogues (L1_m8 for DMO and L1_m9 for the hydrodynamical version).

For the DMO simulations, the difference between L1_m10 (L1_m9) and L1_m8 is about 2% (1%) across the explored mass range. All subhalo finders show essentially the same convergence rate, although VELOCraptor and ROCKSTAR bracket the extremes: VELOCraptor agrees the best between different resolutions and ROCKSTAR the worst. While differences are small for DMO, the picture changes dramatically for hydrodynamical simulations. There is now a substantial difference in the M_{200c} mass function below $\approx 10^{14} M_{\odot}$ between the L1_m10 and L1_m9 simulations, regardless of the subhalo finder.

One caveat to consider when discussing convergence of the M_{200c} mass functions in the hydrodynamical FLAMINGO simulations is whether the actual properties of galaxies and the circumgalactic medium remain consistent across resolutions. The differences could be not due to issues in the subhalo finding, but rather due to changing properties of the haloes themselves. As a matter of fact, the gas fractions within R_{500c} are higher in L1_m10 (Fig. 10 of Schaye et al. 2023) than in L1_m9 below $M_{500c} \approx 3 \times 10^{13} M_{\odot}$. This entails that more gas and dark matter is enclosed within the circumgalactic medium of the haloes below the aforementioned mass scale. As $M_{200} > M_{500}$, the mass scale where the differences start to appear is higher. Hence, the fact that the subhalo finders find an enhancement in L1_m10 relative to L1_m9 is not entirely unexpected.

Nonetheless, two differences unrelated to the above discussion are worth highlighting. The first one is that ROCKSTAR finds fewer low mass haloes at higher resolution, a trend opposite to the one found for the other three subhalo finders. This behaviour is likely caused by the difficulties it encounters when running on hydrodynamical simulations. The second difference is that VELOCraptor now appears to converge at a slightly slower rate than HBT-HERONS and Subfind, both of which exhibit similar convergence properties.

We conclude this subsection by noting that the differences we find in M_{200c} also extend to other spherical overdensity apertures, like M_{500c} . As the choice of which halo mass function to use has important consequences for predictions relevant to ongoing and upcoming cosmological probes (e.g. cluster counts; Kugel et al. 2025), choos-

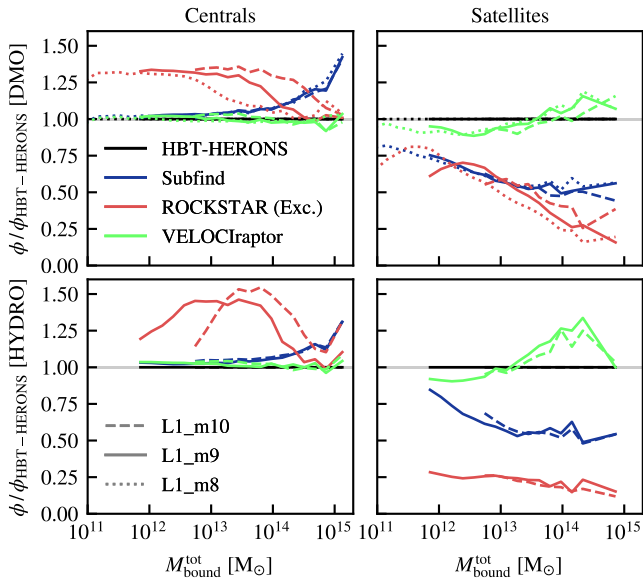


Figure 6. Number density of central (left column) and satellite (right column) subhaloes as a function of their bound total mass. The top panels show the results for the DMO versions of the simulation, and the bottom ones for the hydrodynamical versions. Each coloured line indicates the mass function found using a different subhalo finder, which are expressed relative to the one found using HBT-HERONS at the same resolution. Different resolutions are indicated by the styles of the lines. Only the mass range corresponding to masses greater than the equivalent of 100 DMO dark matter particles (at a given resolution) is shown. Note that for the purposes of this comparison, we modified ROCKSTAR to assign masses exclusively, which is not the default way in which it is run. See Fig. E2 for the plot corresponding to an inclusive mass assignment, in which the differences become much larger between ROCKSTAR and the other subhalo finders.

ing one subhalo finder over the other will likely affect cosmological inferences. We also stress that the convergence properties of a given subhalo finder are insufficient to determine which subhalo finder provides ‘better’ results. As we showed here, even though all subhalo finders share similar convergence properties for the DMO simulations, they converge to different answers. As we will show later on, the convergence to different answers also affects the subhalo bound mass functions and their radial distribution within a halo.

4.2.2 Bound subhalo mass functions

We now shift our attention to the mass bound to subhaloes. We compute it by summing the masses of all particles bound to a given subhalo, which is information provided separately by each structure finder. As the bound mass is measurable for satellite and central subhaloes, we show both of their bound mass functions in Fig. 6.

The differences across subhalo finders in the bound mass functions are larger than for the M_{200c} mass functions. Instead of differing by 5% to 10%, differences now reach upwards of 50% for both centrals and satellites. The larger changes are expected due to this mass definition depending more strongly on the assumptions and methodology that each finder uses, e.g. how well they separate satellites from centrals, whether they use an iterative unbinding scheme, etc.

Focusing first on the differences between Subfind and HBT-HERONS, Subfind finds more massive central subhaloes at $M_{\text{bound}}^{\text{tot}} \geq 10^{13} M_{\odot}$, with the most massive being 40% more massive in Subfind. As the differences between them are much smaller for the M_{200c} mass functions, the differences are driven by how

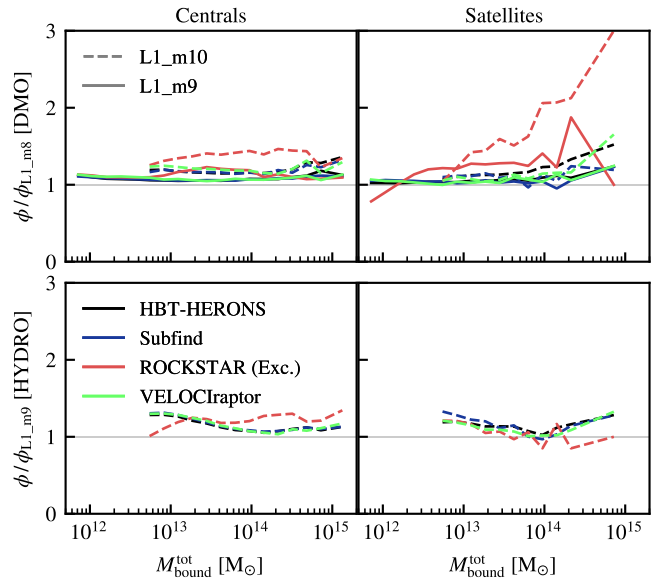


Figure 7. Similar to Fig. 6, but showing how the M_{bound} mass function converges across resolution levels using different subhalo finders. The mass functions for a given subhalo finder are normalised to the mass function obtained from the same subhalo finder using the highest resolution simulation available for that box (L1_m8 for DMO and L1_m9 for hydro). Note that for the purposes of this comparison, we modified ROCKSTAR to assign masses exclusively, which is the way mass is assigned by the other subhalo finders, but it is not ROCKSTAR’s default behaviour.

much bound mass each central subhalo is assigned. Indeed, as we saw qualitatively in Fig. 2, HBT-HERONS is better at separating satellites from centrals than Subfind. This is both because SUBFIND misses more satellites, and because it is more likely to remove mass from their outskirts (Han et al. 2012). This means that some of the mass which HBT-HERONS finds to be bound to satellites is instead assigned to centrals in Subfind. Thus, for the same central, one typically expects to have more bound mass in Subfind. Conversely, the Subfind satellite bound mass functions are suppressed by up to 50% at fixed M_{bound} relative to HBT-HERONS. The differences for centrals and satellites remain consistent with resolution and whether or not the simulation uses hydrodynamics.

The bound mass function of centrals in VELOCiraptor is very similar the one found by HBT-HERONS. There is a minor trend with bound mass where, relative to HBT-HERONS, VELOCiraptor overestimates the mass function by 5% at the low mass end and underestimates it by the same amount at the high mass end. For satellites, larger differences appear relative to HBT-HERONS, but they remain the most consistent out of the subhalo finders used in this work. Similar to the central bound mass function, there is a trend with mass, but it is now reversed and more evident. The suppression at the low mass end is partially caused by VELOCiraptor not identifying small subhaloes and assigning less mass to them. At higher masses, the disagreement is caused by the definition of central. In HBT-HERONS, the central is the most massive subhalo within a FoF group. This is not necessarily the case in VELOCiraptor, as the central is the top level structure in the 3D FoF before doing any phase-space searches. This means that satellites can be more massive than centrals in certain cases.

ROCKSTAR differs strongly in its central bound mass relative to the other subhalo finders, but the interpretation is complicated by its definition of central subhaloes differing from the other subhalo finders. A more consistent approach would modify the central population that ROCKSTAR finds to be more in line with the other three finders

(e.g. Gómez et al. 2022). With this difference in mind, the boost relative to HBT-HERONS at low masses is likely driven by satellites in HBT-HERONS being counted as centrals by ROCKSTAR. Comparing the high mass end is more informative, as the contributing number of satellites is expected to be low for all subhalo finders. We see that it agrees well with HBT-HERONS, although the range of masses where both agree is sensitive to the resolution of the simulation.

Shifting to the satellite population, ROCKSTAR results in the most suppressed bound mass functions relative to HBT-HERONS. The satellite high mass end is the least populated out of the four finders, although this is in part due to ROCKSTAR classifying more subhaloes as centrals. The number densities of low mass satellites are comparable to Subfind, and both are lower by $\approx 25\%$ compared to HBT-HERONS and VELOCIRaptor in the DMO simulations. For the hydrodynamical simulations, the suppression relative to HBT-HERONS is as severe as $\approx 75\%$, a consequence of including gas and stars to run 6D FoF. Overall, both the central and satellite bound mass functions depend more strongly on resolution for ROCKSTAR than is the case for the rest of finders. Since this analysis is based on a modified version of ROCKSTAR to enable exclusive mass assignment (i.e. a particle can only be bound to a single subhalo at a time), we re-do the same analysis based on the default version of ROCKSTAR in Appendix E. Using ROCKSTAR's inclusive mass definition results in much larger differences in the number densities of subhaloes at a fixed M_{bound} relative to the other subhalo finders. The differences in the number densities increase as the bound mass of the subhalo increases, with $10^{15} M_{\odot}$ subhaloes reaching number densities that can be higher by a factor of 10 in ROCKSTAR than in the other subhalo finders.

Given the strong changes in the ratio of mass functions as a function of resolution for ROCKSTAR, we proceed to look at the convergence of the bound mass functions. In other words, how well each subhalo finder approaches the results it obtains at the highest resolution we have available for each box. We show this convergence test in Fig. 7.

Generally, the bound mass of centrals is larger in lower resolution simulations for all subhalo finders. This trend is caused by the fact that fewer satellite subhaloes are resolved at lower resolutions. As the resolution increases, they are found as resolved satellites and hence the central loses out on that bound mass. For satellites, the trend appears to be similar, except for satellites in the hydrodynamical simulation found by ROCKSTAR. We believe this is because unresolved substructures (e.g. satellites of satellites) become resolved, and hence remove bound mass from its parent satellite.

ROCKSTAR differs much more across resolution levels than the other subhalo finders. For example, for the other three subhalo finders the L1_m10 central bound mass function differs by no more than 25% from L1_m8. In contrast, ROCKSTAR is a factor of three higher than the values it finds at L1_m8. We remind the reader that this analysis is based on our implementation of exclusive mass definition within ROCKSTAR. We also explored the convergence of M_{bound} using the default (inclusive mass) version of ROCKSTAR. We found that its convergence properties are comparable to the results of other subhalo finders, if not marginally better. The slight improvement when using inclusive masses is due to the fact that centrals do not lose mass as satellites become resolved, whereas using an exclusive mass definition leads to the reassignment of mass from central to satellite subhaloes.

The hydrodynamical versions may appear to converge better at first glance. However, the ratios are between two consecutive resolution levels (L1_m10 to L1_m9), whereas the DMO ones are always relative to L1_m8. Still, we observe the same trends as we did in the DMO versions, although satellites in ROCKSTAR remain consistently low regardless of resolution.

We conclude this subsection by noting that differences in the mass function do not only reflect the performance of individual subhalo finders in distinguishing satellites from centrals, but also the definition of what a subhalo is. This is caused by different criteria for how resolved subhaloes are selected. HBT-HERONS, Subfind and VELOCIRaptor do iterative unbinding and keep those subhaloes with more than a threshold number of particles. ROCKSTAR only does one unbinding iteration and retains in the catalogue those subhaloes whose bound particle fraction relative to the initial 6D FoF groups is above a threshold. Changing the threshold will change the type of objects included in ROCKSTAR catalogues. For example, a stream may remain coherent in 6D phase space, despite having few bound particles. Thus, if the value of the threshold is set low enough, these types of objects will be included in ROCKSTAR catalogues. By virtue of the definition used by other subhalo finders, these structures will generally always be excluded, although VELOCIRaptor can also be used to find streams (e.g. Elahi et al. 2011).

4.2.3 Maximum circular velocity functions

Besides the subhalo mass function, it is also of interest to quantify the number of subhaloes as a function of their maximum circular velocity, as given by equation (10). The maximum circular velocity is expected to be less sensitive to the choice of subhalo finder than the bound mass of a subhalo (e.g. Knebe et al. 2011), since its value is less reliant on how the edge of the subhalo is defined. As a large fraction of mass is located around the outskirts of subhaloes, even if the subhalo core is found consistently across subhalo finders, slightly changing the edge of the subhalo may propagate to larger changes in M_{bound} than the corresponding changes in V_{max} .

To explore if the differences we discussed in §4.2.2 only reflect differences in the subhalo outskirts, or if they are also attributable to changes in the central mass distribution, we show in Fig. 8 the subhalo number densities as a function of their V_{max} . In order to study a similar mass range as shown in Fig. 6, $M_{\text{bound}} \in [10^{11}, 10^{15}] M_{\odot}$, we measure the mean V_{max} of subhaloes whose bound masses are near the upper and lower limits of M_{bound} . We then round the values to reach the upper and lower limits we use, $V_{\text{max}} \in [100, 1500] \text{ km s}^{-1}$. To identify the lowest value of V_{max} that we show for each resolution level, we use the 99th percentile of V_{max} values for subhaloes whose bound masses are less than the equivalent mass of 100 DMO dark matter particles.

The clearest difference is the improvement in the agreement between Subfind and HBT-HERONS, but differences remain. The abundance of the most massive central subhaloes at a fixed V_{max} is within $\approx 30\%$, whereas differences based on M_{bound} were within $\approx 50\%$. On the other hand, the agreement between VELOCIRaptor and HBT-HERONS does not substantially improve for central subhaloes. In fact, the differences increase for satellite subhaloes, so using V_{max} instead of M_{bound} does not automatically result in better agreement.

ROCKSTAR has systematically suppressed number densities for the centrals with the highest V_{max} , despite the relatively good agreement for the highest M_{bound} central subhaloes (see the top right panel of Fig. 6). One possibility that could explain these lower V_{max} values is that ROCKSTAR uses the centre of mass of a subhalo as the centre of the spherical aperture used to compute V_{max} . If the centre of mass is offset from the true density peak of its centre, V_{max} might be underestimated. Another explanation is that there is more substructure in the core of central subhaloes compared to all of the other subhalo finders, which we explore in §4.3. If the core of a central subhalo has less bound mass because it is instead assigned to its substructure,

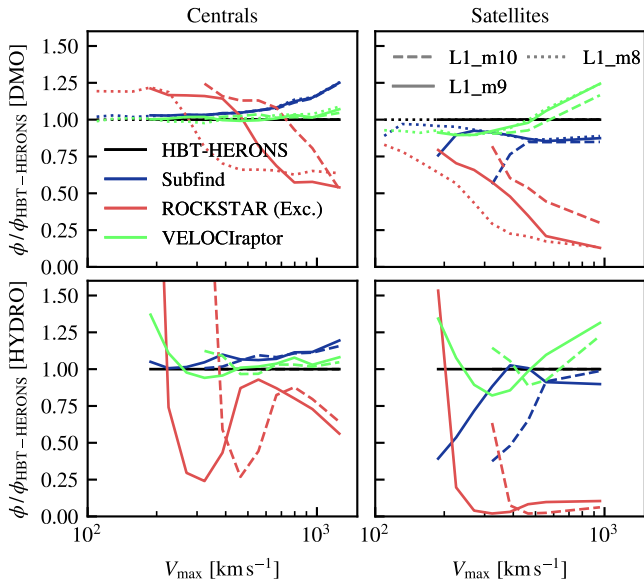


Figure 8. Similar to Fig. 6, but the distributions are based on the V_{\max} values of subhaloes. The lowest V_{\max} we show at a given resolution corresponds to the 99th percentile of V_{\max} values for subhaloes with bound masses that correspond to fewer than 100 DMO dark matter particles. Note that for the purposes of this comparison, we modified ROCKSTAR to assign masses exclusively, which is the way mass is assigned by the other subhalo finders, but it is not ROCKSTAR’s default behaviour. See Fig. E3 for the plot corresponding to an inclusive mass assignment, which leads to smaller differences than the version presented here.

it will lower the central subhalo V_{\max} . Similar to what we find for central subhaloes, the satellite V_{\max} values in ROCKSTAR are also suppressed compared to all other subhalo finders.

We note that these findings are based on our implementation of exclusive mass assignment, but we show the equivalent plot that uses the default (inclusive mass) implementation of ROCKSTAR in Fig. E3. Using an inclusive mass definition results in less discrepant number densities between ROCKSTAR and HBT-HERONS at the high V_{\max} end of satellite subhaloes, although they still differ by $\approx 50\%$. The better agreement is due to satellites having larger V_{\max} values in the inclusive ROCKSTAR mass definition, compared to those found using an exclusive mass assignment. Hence, the number densities are not as suppressed as when using an exclusive mass assignment, which reached differences of up to $\approx 75\%$.

The hydrodynamical versions show the same qualitative trends as the DMO simulations. Subfind and HBT-HERONS agree better for the highest V_{\max} subhaloes than for the corresponding M_{bound} function, although the number density of the lowest V_{\max} satellites are more suppressed in Subfind relative to HBT-HERONS than in the DMO simulations. VELOCiraptor and HBT-HERONS agree less well than a comparison based on M_{bound} . The number densities based on ROCKSTAR are heavily suppressed relative to other subhalo finders, due to its difficulties in analysing hydrodynamical simulations. This last difference is present regardless of whether we use inclusive or exclusive masses (see the bottom right panel of Fig. E3).

To summarise the findings discussed within this subsection, we have shown that a variety of commonly used mass metrics can result in widely different mass functions depending on the chosen subhalo finder. Halo masses based on a spherical overdensity, e.g. M_{200c} , are the most consistent out of the three we have explored here. However, differences of up to 10% appear in the number densities of low

M_{200c} haloes, which are largely driven by the purely theory-based definition of what constitutes a central subhalo. Choices concerning whether to assign a single central per FoF group (HBT-HERONS, Subfind and VELOCiraptor) or based on a spherical exclusion criteria (ROCKSTAR), alongside additional choices involved in either of these two approaches (e.g. FoF linking length and definition of spherical exclusivity), all contribute to different definitions of central subhalo populations. Quantifying subhalo masses using M_{bound} or V_{\max} results in even more discrepant mass functions compared to using M_{200c} . We also find that using V_{\max} as a mass proxy instead of M_{bound} does not necessarily result in a better agreement across finders. Lastly, the inclusion of hydrodynamics can have severe effects on the capabilities of finding subhaloes, with the most extreme example being ROCKSTAR.

4.3 Abundance and radial distribution of satellite subhaloes

One of the main use cases of subhalo finders is to disentangle satellite subhaloes from the central subhalo that hosts them. As we saw from the example discussed in §4.1, this does not always work as intended. The reason why subhalo finders fail to identify satellites is varied, and reflects the underlying algorithm they use. Density-based finders are known to struggle when there is insufficient contrast between adjacent density peaks (e.g. Behroozi et al. 2015). Phase space finders also struggle if the subhalo is severely tidally distorted (e.g. Mansfield et al. 2024). As these properties correlate with the environment the subhalo is in, e.g. when undergoing a close pericentre passage, there may be a bias in finding subhaloes that varies as a function of the distance to its host and their relative masses.

Given the above, a natural test of how well subhalo finders perform is to compare the abundance and distributions of satellites. In this subsection, we explore several relations that concern both aspects. We begin by looking at the subhalo number density in the outskirts of central subhaloes (§4.3.1). We then examine how the shape of the subhalo number density distribution varies as a function of host M_{200c} (§4.3.2) and satellite-to-host bound mass ratio (§4.3.3). As we measure the last two statistics at a fixed resolution level, haloes with lower M_{200c} or satellites with lower satellite-to-host bound mass ratios are less well sampled by particles than those with correspondingly larger values. In other words, resolution trends may masquerade as mass trends. To disentangle one from the other we also present convergence tests.

The central subhalo population is significantly different for ROCKSTAR compared to the other subhalo finders (§4.2.1). To prevent changes in the definition of central from driving differences in the radial distributions, we count all subhaloes at a given distance regardless of whether they are classified as centrals or satellites. Throughout this subsection, we only take into account subhaloes with a bound mass that is at least 100 times the mass of a dark matter particle in the DMO simulations.

4.3.1 Number of subhaloes in the outskirts of central subhaloes

We start the comparison by looking at how many subhaloes there are near R_{200c} of central subhaloes, measured using a bin of width 0.1 dex. This corresponds to approximately $[0.8-1] \times R_{200c}$. Our focus on the outskirts of haloes reflects the fact that we expect the difficulties associated with heavily overlapping or disturbed subhaloes to be less important than in the inner regions. Thus, this test will reveal whether there are already systematic differences in the number of subhaloes in regions expected to be relatively well resolved.

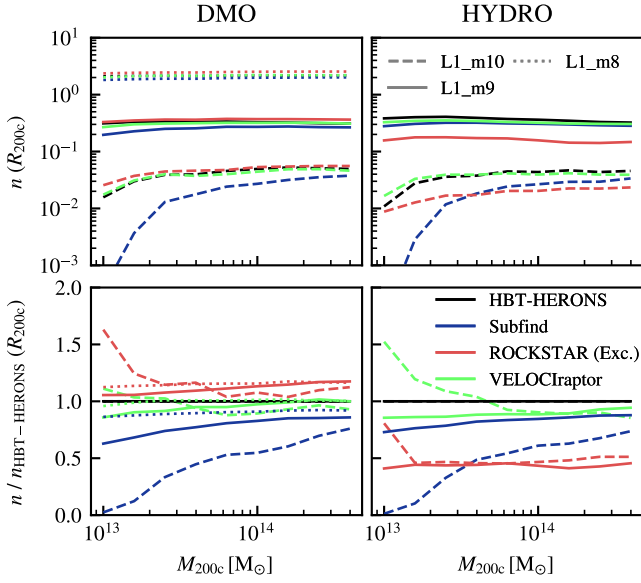


Figure 9. *Top panels:* Mean number density of subhaloes in the outskirts of haloes, as a function of their central M_{200c} mass. The number density is measured by counting subhaloes with a total bound mass greater than 100 DMO dark matter particles in a spherical shell spanning $[0.8 - 1] \times R_{200c}$ of the corresponding host. All subhaloes within the shell are included regardless of whether they are a central or a satellite, in order to minimise differences that are driven purely by the definition of a central. Results from the DMO and hydrodynamical versions of the boxes are shown in the left and right columns, respectively. *Bottom panels:* The same as above, but expressed relative to the number density found by HBT-HERONS. Note that for the purposes of this comparison, we modified ROCKSTAR to assign masses exclusively, which is the way mass is assigned by the other subhalo finders, but it is not ROCKSTAR’s default behaviour.

The mean number density of subhaloes near R_{200c} as a function of the M_{200c} of the host is shown in the top panels of Fig. 9. We show this relation for all resolution levels for which subhalo catalogues are available. For the L1_m9 and L1_m8 simulations, there is little to no dependence of $n(R_{200c})$ on M_{200c} . This is because $n(R_{200c}) \propto N_{\text{sub}} R_{200c}^{-3} \propto N_{\text{sub}} M_{200c}^{-1}$, where N_{sub} is the number of subhaloes enclosed within the spherical shell. Since the number of subhaloes within R_{200} scales approximately linearly with M_{200c} (e.g. Wang et al. 2012), the number of subhaloes in the outskirts also scales linearly with mass, and hence $n(R_{200})$ remains approximately constant. Comparing L1_m9 to L1_m8, we see an upwards shift in the number density of subhaloes, corresponding to more of them being resolved thanks to the increased resolution.

A caveat worth adding is that, when selecting subhaloes according to a fixed subhalo mass limit, a linear relation between the number of subhaloes and M_{200c} is only expected when the subhalo mass limit is far away from the exponential cut-off mass scale of the corresponding subhalo mass function. As we lower the resolution, the mass limit (100 DMO particles) used to select subhaloes increases, resulting in limits that shift closer to the exponential cut-off scale. For the lowest M_{200c} haloes, the mass limit can become comparable to the exponential cut-off scale, thus making them the most susceptible to experience a departure from linearity between M_{200c} and $n(R_{200c})$. Indeed, this could be one of the reasons behind why the subhalo number density no longer remains constant with M_{200c} in the L1_m10 simulation across subhalo finders. As the subhalo mass functions can also differ across subhalo finders, e.g. with the exponential cut off in the subhalo mass function occurring at a lower mass scale or

with a systematic shift in the assigned masses, the departure from $N_{\text{sub}} \propto M_{200c}$ will generally depend on the employed subhalo finder.

To explore the differences in the measured number density of subhaloes across subhalo finders, we show in the bottom panels of Fig. 9 their $n(R_{200c})$ relative to that of HBT-HERONS. For all of the DMO simulations, Subfind always finds the lowest number density out of the four subhalo finders. The suppression relative to HBT-HERONS is resolution dependent. At the high mass end, the ratio increases from 0.75 for L1_m10 to 0.87 for L1_m8. For lower masses, the number varies from virtually zero to 0.87 that of HBT-HERONS. At the other end of the spectrum, ROCKSTAR consistently finds the largest subhalo number density across all resolutions of the DMO simulations, around 20% more than the results based on HBT-HERONS. Out of the three alternative subhalo finders, VELOCItaptor finds values of $n(R_{200c})$ that are most consistent with HBT-HERONS, regardless of the resolution.

We now shift our attention to how the subhalo number densities change in the hydrodynamical versions of FLAMINGO, which are shown in the top right panel of Fig. 9. The clearest change is that ROCKSTAR is no longer the subhalo finder that consistently finds the highest subhalo number density. In fact, for L1_m9, it finds the lowest densities out of all subhalo finders. As discussed previously, this is driven by the fact that ROCKSTAR struggles to find subhaloes when linking particles regardless of their type. Another difference relative to the DMO versions is that the number density of subhaloes tends to be higher across M_{200c} for the L1_m9 hydrodynamical version, according to HBT-HERONS, Subfind and VELOCItaptor.

The increase in the number of satellites may be surprising. At Milky Way- (MW) mass scales, which many radial distribution studies focus on, the net change caused by the addition of hydrodynamics is a decrease in the number of satellite subhaloes (e.g. Samuel et al. 2020). This is attributed to a combination of their hindered growth due to early mass loss (e.g. Sawala et al. 2017) and stronger tides due to the presence of a baryonic disc in the host (e.g. Garrison-Kimmel et al. 2017). Evidently, extrapolating those results to the mass scales we study here would yield an incorrect expectation.

What could cause the difference between the outcome resulting from the inclusion of baryons for MW scales and cluster scales? The efficiency of galaxy formation varies with mass, so satellites in clusters correspond to the mass range expected to harbour sufficient baryons to induce a contraction of their DM subhalo. Indeed, as we already saw in Fig 2, subhaloes in the hydrodynamical simulations clearly have denser cores than in the DMO simulation. As denser centres make subhaloes more resilient to gravitational tides (e.g. Peñarrubia et al. 2010), they are less likely to be stripped to masses below the resolution of the simulation. On MW-mass scales, the masses of satellites correspond to the regime of inefficient galaxy formation, where contraction is expected to be less important (and expansion may even occur).

The level of agreement between subhalo finders changes when looking at the hydrodynamical simulations. In particular, Subfind and HBT-HERONS agree to within $\approx 10\%$ for the L1_m9 hydrodynamical simulation, i.e. as well as for the L1_m8 DMO simulation. On the other hand, ROCKSTAR now underpredicts the number of subhaloes relative to HBT-HERONS. As before, we note that this is likely driven by our choice of linking all particle types for ROCKSTAR. This highlights once again the importance of taking proper care when analysing hydrodynamical simulations using subhalo finders that were developed for DMO simulations.

As discussed earlier, relative to the DMO simulation, the number of subhaloes increases for all subhalo finders but ROCKSTAR. However, the increase is not uniform across finders. In particular, the increase

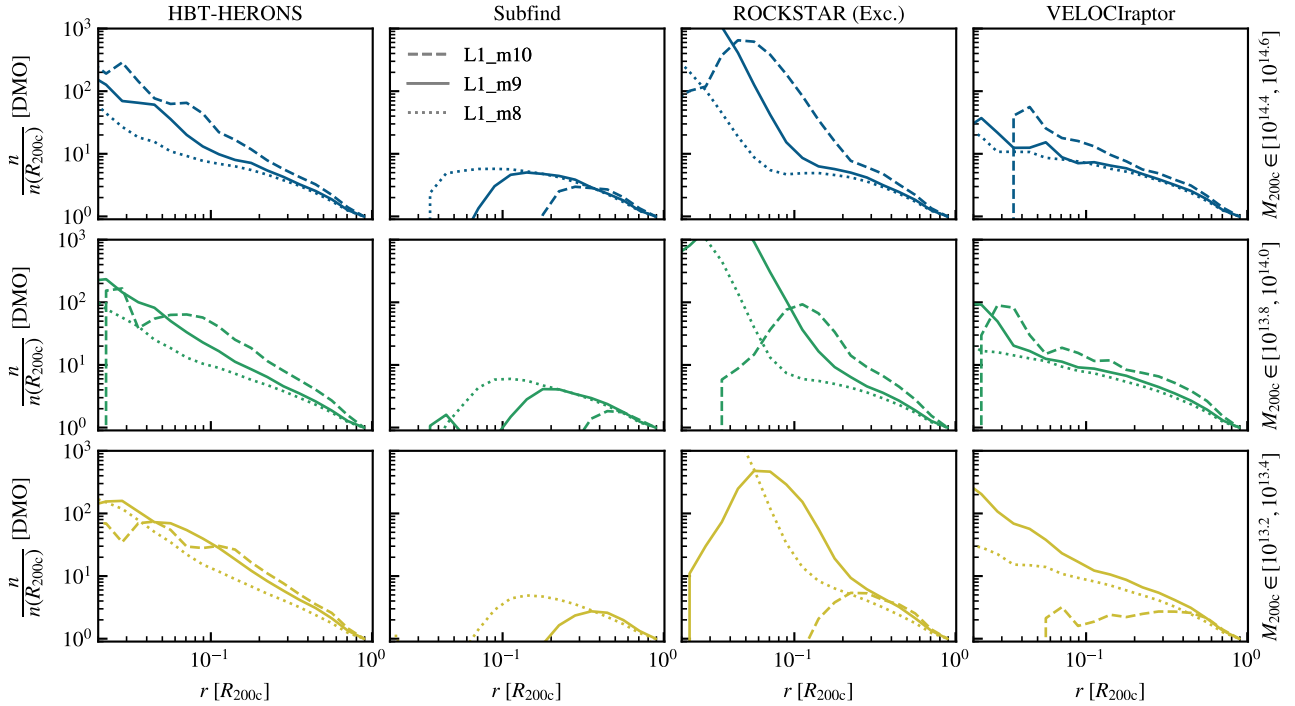


Figure 10. Mean subhalo number density as a function of normalised distance to the central subhalo for different DMO resolutions (different line styles) and averaged in different bins of M_{200c} (different line colours and rows). The values of M_{200c} that bracket each bin are indicated on the right hand side of each corresponding row, and encompass 0.2 dex in M_{200c} and are spaced 0.6 dex from each other. Each column corresponds to the results found by a different subhalo finder. The number densities are normalised to the value found by each subhalo finder in the outermost radial shell for each resolution and mass bin. We count all subhaloes whose bound mass is at least 100 times the DMO particle mass, regardless of whether they are classified as centrals or satellites. This choice is made to minimise differences that are driven purely by the definition of a central. Note that for the purposes of this comparison, we modified ROCKSTAR to assign masses exclusively, which is the way mass is assigned by the other subhalo finders, but it is not ROCKSTAR’s default behaviour.

in the number of Subfind subhaloes at R_{200c} is the largest. The net effect is better agreement between HBT-HERONS and Subfind for L1_m9 hydro than for the highest resolution DMO simulation we have (L1_m8). The improvement is likely caused by the fact that subhaloes become denser in the hydrodynamical simulations, which helps Subfind identify density peaks more easily.

4.3.2 Radial distributions as a function of host halo mass

Another important property of subhalo populations is how they are distributed within their host haloes. In this subsection, we measure their distribution by counting how many subhaloes are present within a given spherical shell. We use 20 shells whose edges are logarithmically spaced between $[0.01 - 1] \times R_{200c}$. A subhalo is assigned to a shell based on where its centre is located. We then divide by the volume of the shell to obtain the subhalo number density as a function of distance to the centre of the host.

As the satellite distribution of an individual halo can be noisy and not representative of the mean trend, we average the number density distributions in nine M_{200c} bins between 10^{13} and $10^{15} M_{\odot}$. All but the highest M_{200c} bin span 0.2 decades in mass. The highest mass bin is enlarged to 0.4 decades to increase the number of centrals it contains to about 755¹¹.

In the preceding subsection, we found that the number density

of subhaloes differs between subhalo finders even near R_{200c} . This means that differences in the distributions will appear due to differences in the normalisation. In this subsection, we are more interested in how the shape of the distribution changes between finders. Therefore, to decouple the effect of different numbers of subhaloes found across subhalo finders, we normalise the subhalo number densities by the number density found by each subhalo finder in the outermost spherical shell (spanning $[0.8 - 1] \times R_{200c}$).

An important caveat is that, since we are comparing the radial distribution of subhaloes in a simulation using a fixed particle mass, bins with lower values of M_{200c} correspond to less well resolved systems. Therefore, an apparent trend with M_{200c} may just be a trend with resolution. To help us interpret the trends and differences between subhalo finders, we first examine how the DMO radial distributions change across the L1_m10, L1_m9 and L1_m8 resolutions. The corresponding distributions are shown in Fig. 10, which are measured in the manner described above for a subset of the M_{200c} bins we will explore.

Focusing first on the normalised subhalo number densities from the L1_m10 simulation, we see that the shapes are very different at a fixed M_{200c} depending on the subhalo finder used to derive them. The shapes for Subfind are non-monotonic and peak at a radius that decreases as M_{200c} (or the number of particles within R_{200c}) increases. On the other end of the spectrum, using HBT-HERONS generally results in a monotonic number density for the plotted radial range across all M_{200c} . ROCKSTAR and VELOCiraptor show a behaviour that can be more similar to either Subfind (e.g. $M_{200c} \in [10^{13.2}, 10^{13.4}] M_{\odot}$ in L1_m10) or HBT-HERONS (e.g. $M_{200c} \in [10^{14.4}, 10^{14.6}] M_{\odot}$ in L1_m10).

¹¹ There are small differences in the number of centrals across subhalo finders in the highest M_{200c} bin due to different M_{200c} being measured for the same haloes (e.g. Fig 3).

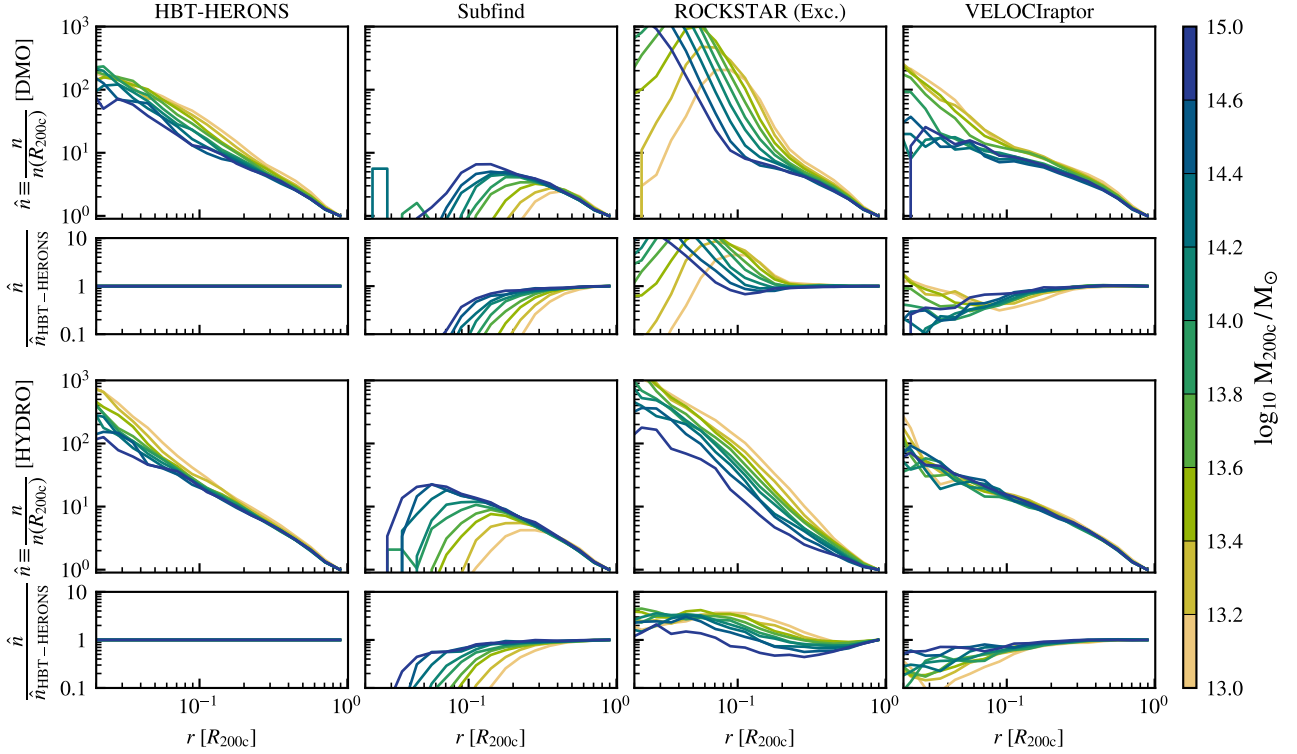


Figure 11. Similar to Fig. 10, but shown for the L1_m9 DMO and hydrodynamical simulations and for a larger range of M_{200c} halo masses. *Top panels:* the radial distributions found in the DMO version of the simulations. The secondary panel shows the ratio of the normalised subhalo number densities of each subhalo finder relative to the values found in HBT-HERONS *Bottom panels:* Same as the top panels, but for the hydrodynamical version of the simulations.

Looking at how the normalised subhalo number density distributions change as the resolution increases, we see that the distributions converge differently across subhalo finders. For Subfind, the radius below which no substructure is found shifts to smaller distances. The normalised subhalo number densities found by Subfind always agree well across resolutions beyond the radius at which the normalised number density peaks. This scale provides a natural ‘convergence’ radius. On the other hand, the other three subhalo finders do not exhibit a clear ‘convergence’ radius, as increasing the resolution results instead in increasingly flatter shapes for $n(r)/n(R_{200c})$. We can clearly see that this change from L1_m9 to L1_m8 is primarily driven by a decrease in the normalised number density of subhaloes in the central regions.

How can one make sense of the fact that subhalo finders that find more subhaloes, e.g. HBT-HERONS, exhibit a decrease in the normalised number density of subhaloes as resolution increases? It all has to do with how massive (relative to the host halo) the largest resolvable satellites are. At a fixed host M_{200c} , increasing the resolution increases the number of particles that sample its virial region. Hosts with $M_{200c} \in [10^{13.2}, 10^{13.4}] M_{\odot}$ have approximately 300 to 500 particles within R_{200c} at the L1_m10 resolution. We can estimate the minimum resolvable satellite-to-central mass ratio if we assume all particles within R_{200c} are bound the central or a single satellite subhalo. For our selection cut of 100 bound particles, the satellite-to-central mass ratio is $N_{\text{sat}}/(N(\leq R_{200c}) - N_{\text{sat}}) \approx 100/(500 - 100) = 0.25$. Thus, lowering the resolution increasingly biases the radial distributions to be more dominated by major mergers. As we show in the following subsection, the high mass end of the satellite population is more concentrated towards the centre in HBT-HERONS. This explains why the shapes are steeper for a lower resolution simulation than for a higher resolution one.

We also show in §4.3.3 that Subfind struggles to identify satellites with masses above $\approx 0.1\%$ that of their host, either by not finding the subhalo itself or by removing so much mass from it that it falls below our 100 DMO dark matter particle mass cut. This makes its trend with resolution different to the other subhalo finders. Since changing M_{200c} at a fixed resolution is equivalent to changing the number of particles within R_{200c} , we expect that the resolution trends we just discussed will also appear as mass trends. In other words, we expect that lowering M_{200c} increasingly biases the radial distributions to be more dominated by major mergers and hence more radially concentrated for HBT-HERONS, ROCKSTAR and VELOCItaptor. For Subfind, the difficulty in finding massive satellites will result in more suppressed subhalo number densities as M_{200c} is lowered.

In Fig. 11, we can now compare the performance of different subhalo finders at the same resolution level and different M_{200c} . The number density of subhaloes generally increases towards the centre, except when there is a clear cut-off due to resolution-dependent issues related to subhalo finding. Only Subfind and ROCKSTAR show a drop at small radii, suggesting they perform worse in the inner regions than HBT-HERONS and VELOCItaptor at the same resolution level. Interestingly, ROCKSTAR exhibits a peak in the number density of subhaloes at radii slightly larger than where their density sharply decreases. We attribute this increase to resolution-dependent spurious subhaloes being identified in poorly resolved regions, which are prone to noise in the particle distribution. The chosen bound fraction threshold (0.5) was therefore unable to remove them. Further post-processing steps could help remove them if they are indeed spurious (e.g. Behroozi et al. 2013b), but we intentionally do not use any additional tools external to the subhalo finders themselves.

The level of agreement between subhalo finders in the shapes worsens for lower M_{200c} , i.e. in more poorly sampled haloes. This is par-

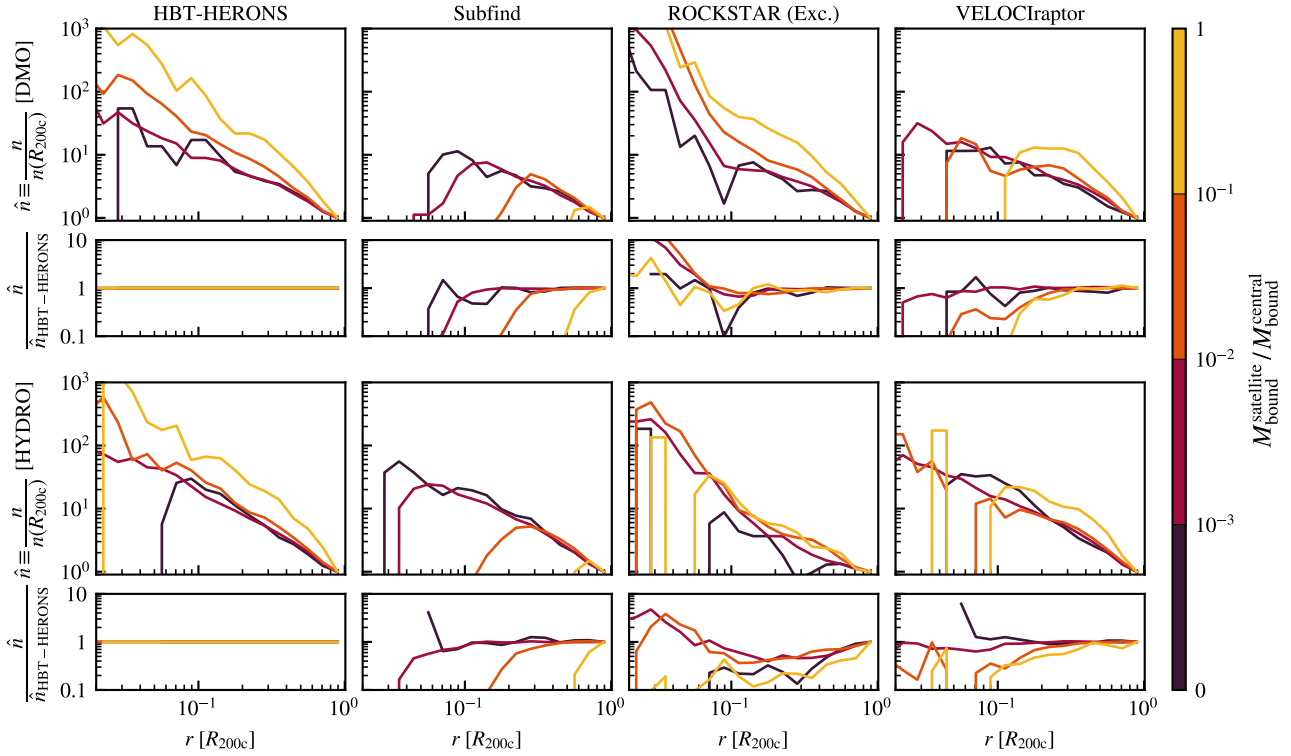


Figure 12. Similar to Fig. 11, but the subhalo number density distributions are shown for bins of different satellite-to-host bound mass ratios (different line colours) in the L1_m9 simulation measured for haloes with $M_{200c} \in [10^{14.6}, 10^{15.0}] M_{\odot}$. *Top panels:* the radial distributions found in the DMO version of the simulations. The secondary panel shows the ratio of the normalised subhalo number densities of each subhalo finder relative to the values found in HBT-HERONS. *Bottom panels:* Same as the top panels, but for the hydrodynamical version of the simulations.

ticularly prominent for Subfind, as it agrees well with HBT-HERONS beyond $0.2R_{200c}$ for the highest M_{200c} bin we consider. For the lowest M_{200c} bin, it only agrees with HBT-HERONS beyond $0.6R_{200c}$. This trend is less prominent for VELOCItaptor, as the agreement with HBT-HERONS is always good beyond $0.3R_{200c}$. ROCKSTAR agrees well beyond $0.3R_{200c}$ but within $r \ll 0.1R_{200c}$, the subhalo number density in ROCKSTAR is more than a factor 10 larger than for HBT-HERONS. The distance below which the normalised number densities of subhaloes disagree is likely driven by how well different subhalo finders perform in poorly resolved regions. Recall that even if the shapes agree, the overall normalisation generally does not (see Fig. 9).

HBT-HERONS, ROCKSTAR and VELOCItaptor do not exhibit good agreement between the normalised subhalo number density distribution across haloes of different M_{200c} (i.e. resolution). However, the shapes of the distributions and trends with M_{200c} differ between them. Generally, they find more substructure at smaller distances than Subfind, which is expected since density-based finders can struggle to cleanly separate (or identify) subhaloes that are in close proximity, leading to a substantial change in their properties and hence whether they are selected at a given cut or not. HBT-HERONS finds the highest number density across all the shown M_{200c} bins, as it is the only finder that measures an approximately monotonic relation in the plotted radial range. Both ROCKSTAR and VELOCItaptor exhibit a cut-off in the number density that shifts to larger normalised distances as M_{200c} decreases. Similarly to Subfind, this occurs because the subhalo finders are unable to find substructure interior to this radius.

We now shift our attention to how the radial distributions change in the hydrodynamical simulations (bottom two rows of Fig. 11). The shapes differ in several aspects from the DMO ones. The number

density profiles become steeper across all subhalo finders and in all host M_{200c} bins. This results in normalised number densities that are higher by factors of two to tens at the smallest radii we explore here. Since the number of subhaloes near R_{200c} also increases (see Fig. 9), this implies there are more subhaloes throughout the virial regions of haloes.

Previous studies found a similar change between DMO and hydrodynamical simulations (e.g. Haggard et al. 2021; Riggs et al. 2022). Some explanations were put forward in Haggard et al. (2021) to explain the cause behind the increase in abundance. One explanation was that their density-based subhalo finder (AHF; Gill et al. 2004; Knollmann & Knebe 2009) finds subhaloes more effectively once baryons are included. Although we find this to be the case, e.g. Subfind agrees more closely with HBT-HERONS in hydro than in DMO simulations, we see the increase across subhalo finders. Thus, the greater number of subhaloes occurs independently from changes due to the halo finding.

Alternative explanations attribute the difference to longer survival times of subhaloes. As discussed in §4.3.1, subhaloes in FLAMINGO have denser centres than in the DMO simulations, which presumably makes them more resilient to tidal stripping. Riggs et al. (2022) matched subhaloes between their DMO and hydrodynamical counterparts, finding that many subhaloes in the hydrodynamical simulation were indeed missing in the DMO simulation. Interestingly, the subhaloes that were successfully matched were more spatially concentrated in the hydrodynamical simulation. They argued that the fact that the satellites were found closer to the centres of their hosts could also reflect changes in their orbits relative to the DMO simulations. The orbital changes could in principle be caused by a more concentrated gravitational potential of the host, or stronger dy-

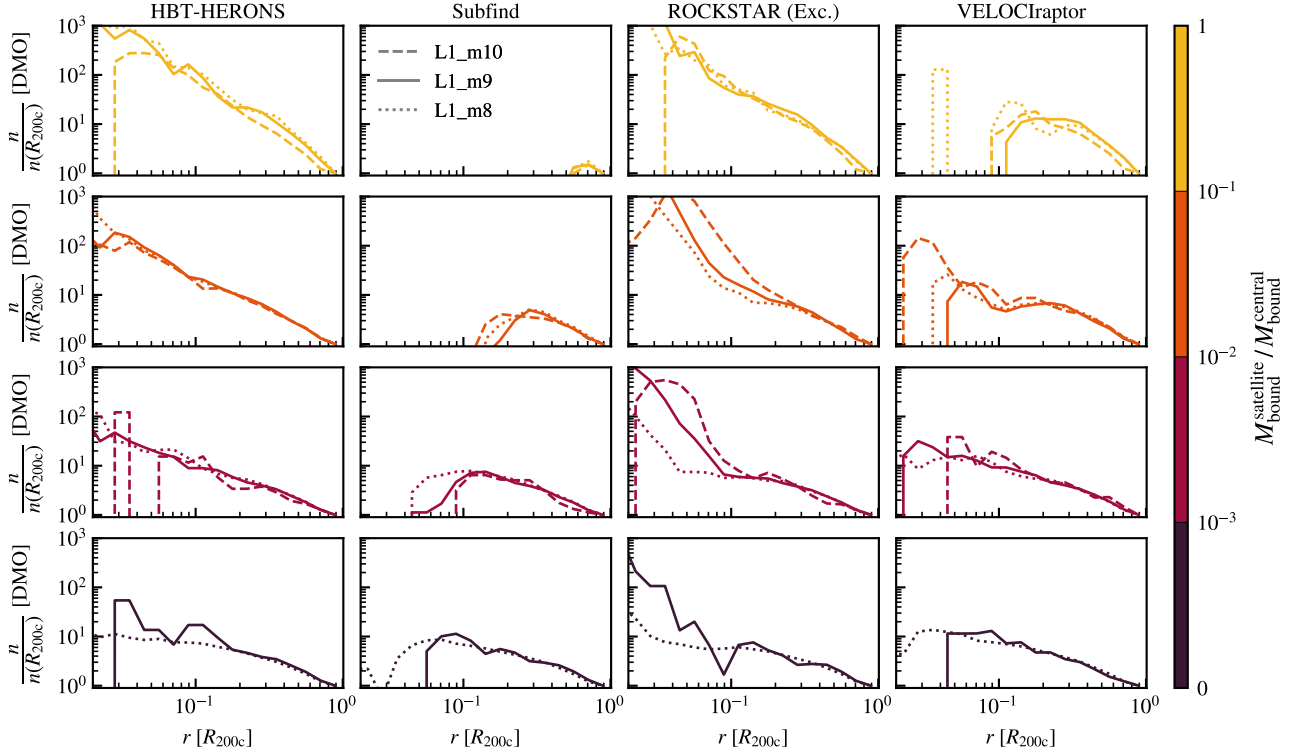


Figure 13. Similar to Fig. 12, but the subhalo number density distributions are now shown for across the three available DMO resolutions (different line styles). Different bins of satellite-to-host bound mass ratios are shown using different colours, as indicated in the colour bar. Note that the L1_m10 simulation has a very undersampled distribution in the lowest bin in $M_{\text{satellite}}/M_{\text{central}}$. For our cut of 100 bound particles, $M_{\text{satellite}} \approx 10^{12} M_{\odot}$. This means only very few satellites will contribute to our measurements, as the bin itself requires $M_{\text{satellite}} \leq 10^{-3} \times [10^{14.6}, 10^{15}] M_{\odot} = [10^{11.6}, 10^{12}] M_{\odot}$.

namical friction due to the increased contrast between the density of the satellite and the background of its host. Determining how the orbits of subhaloes vary in clusters using the self-consistent trees of HBT-HERONS could help shed light on whether friction or the potential is the primary culprit. However, this is beyond the scope of this study.

Another change in the radial distributions is that the dependence on the host M_{200c} (i.e. resolution) is less pronounced for the hydrodynamical simulations. For VELOCItaptor, all mass bins are comparatively similar down to $0.05R_{200c}$. Subfind profile shapes also agree for all mass bins in the regions exterior to where it struggles to find subhaloes ($0.3R_{200c}$ for the lowest M_{200c} bin). For HBT-HERONS, the shapes now agree across M_{200c} masses down to $0.3R_{200c}$. This is likely due to more subhaloes surviving stripping due to their denser cores, and hence the distribution in the hydrodynamical simulation resembles that of a higher resolution DMO simulation.

Another important difference is that, except for ROCKSTAR, different subhalo finders find more consistent results down to smaller radii than for the DMO simulations. For the highest mass bin, VELOCItaptor and HBT-HERONS are within 30% from each other at $0.02R_{200c}$. For DMO, their values disagreed by 80% at this radius. The radius at which Subfind deviates from HBT-HERONS by 50% is $0.02R_{200c}$. In the DMO simulation, this already occurred at $0.1R_{200c}$. The better agreement, beyond longer survival times for subhaloes, is due to the subhalo centres being denser, making it easier to identify density peaks.

4.3.3 Radial distributions as a function of satellite to central mass ratio

In the previous subsection we discussed how different subhalo finders result in different distributions of subhaloes within R_{200c} . This was for the whole population of subhaloes with more bound mass than the equivalent of 100 dark matter particles, regardless of how massive they are relative to the central. However, the distribution of subhaloes can depend on the mass ratio relative to their host, as the importance of various physical mechanisms depends on its value. For example, dynamical friction primarily affects massive satellites, making them sink towards the centre of the host. This can naturally lead to different radial distributions based on the relative mass between satellites and their host.

In Fig. 12, we explore how the subhalo population is distributed according to their satellite-to-central bound mass ratio. The subhalo number densities for each mass ratio bin are divided by the number density found by each corresponding subhalo finder near R_{200c} . For this analysis, we only use the highest M_{200c} bin defined in §4.3.2 ($10^{14.6} M_{\odot} \leq M_{200c} \leq 10^{15} M_{\odot}$), because it contains the largest number of particles within R_{200c} at a fixed resolution. We measure the relative mass between the satellite and its host based on the ratio of their $z = 0$ bound masses, as measured by each subhalo finder. As we are interested in computing a satellite-to-host mass ratio whose upper value is at most 1, we change the definition of central to be the subhalo with the largest M_{bound} within R_{200c} . When performing this re-centering, which results in spatial shifts that are typically of the order of $\sim \mathcal{O}(10)$ kpc, we keep the R_{200c} value estimated from the previous central.

Differences between subhalo finders within a mass ratio bin can

occur in two ways. A subhalo may be completely missing from the catalogue, in which case it does not contribute to any binned measurement. Alternatively, its bound mass may be over- or underestimated. When this happens, it will contribute to a different mass bin relative to its counterpart for a different subhalo finder.

We confirm that the radial distribution functions depend on the satellite-to-host mass ratio, but the direction of the trend differs between subhalo finders. Both HBT-HERONS and ROCKSTAR find high mass satellites to be more spatially concentrated than lower mass ones, as other studies have found in other simulation suites in the past (e.g. Fig. 8 of Han et al. 2018). Subfind and VELOCtraptor find the opposite, with a distinct lack of massive subhaloes within the central parts. VELOCtraptor does find larger numbers of high-mass subhaloes at smaller distances compared to Subfind, likely thanks to its phase-space approach. However, as was shown in Fig. 2, this is sometimes insufficient to separate closely spaced subhaloes.

One may explain the correlation or anti-correlation between satellite mass and spatial concentration using dynamical friction. If the subhaloes remain self-bound as they sink, their number densities will increase at small radial distances, precisely as HBT-HERONS and ROCKSTAR find. If they instead quickly disrupt and mix with their host, their number densities will be suppressed, as Subfind and VELOCtraptor predict.

Based on the evidence we have presented concerning the missing objects in Subfind and VELOCtraptor, we think that the distribution of the most massive subhaloes is indeed more radially concentrated than for their lower mass counterparts. Previous studies that only used Subfind to study the same relation (e.g. De Lucia et al. 2004; Angulo et al. 2009) reached the opposite conclusion. We attribute this to an incorrect interpretation of systematically biased subhalo catalogues, highlighting the importance of robustly finding subhaloes. Note that the high-mass subhalo population is less numerous than the lower mass one, so the former does not determine the overall distributions when all subhaloes are taken into account.

In Fig. 13 we show that this dichotomy of interpretations is resilient to changes in the resolution. Few significant systematic differences with the resolution of the simulation exist in the normalised subhalo number density distribution across all but the lowest satellite-to-host mass ratios. The fact that the distribution does not become more concentrated as the resolution increases implies that the predictions from different subhalo finders converge to different answers. Based on visual inspection of many examples of missing massive satellites (e.g. §4.1), and the well-known limitations of subhalo finders when subhaloes spatially overlap, we argue that the trends recovered by HBT-HERONS and ROCKSTAR are the most physical.

Lastly, the fact that massive objects are not found means that they may be treated as orphans instead. Tracking orphaned subhaloes is done with the aim of improving the agreement between low- and high-resolution simulations, but tracking the evolution of orphans relies on assumptions that lead to different predictions (e.g. Pujol et al. 2017). It would be best to avoid treating massive objects that are resolvable as orphans, in an attempt to compensate for halo finding problems.

To give a sense of how many particles sample the massive, missing objects, we provide an order of magnitude estimate. The hosts we analyse here have $M_{200c} > 10^{14.6} M_{\odot}$. For the L1_m8 simulation, this means they are sampled with $\approx 10^{6.6}$ particles within R_{200c} . If we assume that the bound mass of the central is similar to its M_{200c} , the highest mass ratio bin we use corresponds to satellites of $\approx 10^5$ particles. In other words, these are objects that should be very well resolved, and yet are missing from some catalogues.

We conclude this subsection by showing in the bottom panels of

Fig. 12 how the number density as a function of satellite-to-host mass ratio bin compares across finders in the hydrodynamical simulations. Similar to what we found in the previous subsection, the agreement between Subfind and HBT-HERONS depends on the mass bin under consideration. The smaller the mass ratio, the more likely the satellite is found by Subfind at small distances. The inclusion of hydrodynamics greatly increases the number of objects found by both, particularly for Subfind. The net effect is better agreement with HBT-HERONS, although Subfind is still unable to find the massive satellites at all radii. For ROCKSTAR, the addition of hydrodynamics makes the normalised subhalo number densities agree less well with HBT-HERONS across all satellite-to-host mass bins, and suppresses the densities relative to ROCKSTAR's own results in the DMO simulations. For VELOCtraptor, the second lowest mass ratio bin (10^{-3} to 10^{-2}) agrees better in hydro than in DMO with the results found by HBT-HERONS, although the agreement for the second highest bin (10^{-2} to 10^{-1}) worsens.

4.4 Two-point correlation functions

The last summary statistic we compare across subhalo finders is the two-point correlation function of subhaloes. As we have seen in the previous subsections, the choice of subhalo finder changes the halo virial mass functions, subhalo mass functions (based on M_{bound} and V_{max}) and the radial distribution of subhaloes. One might thus expect that these differences are reflected in the predicted correlation functions, especially in the radial range where the one halo term dominates.

To explore whether this is the case, we compute the auto-correlation function using the Corrfunc package (Sinha & Garrison 2020). We divide the whole subhalo population into four V_{max} bins, without taking into account whether the subhaloes are centrals or satellites. Our choice to use V_{max} reflects the fact that it is a mass proxy that is less sensitive to the chosen subhalo finder algorithm, compared to M_{bound} . Additionally, observationally it is more accessible than the bound mass of subhaloes.

The resulting correlation functions are shown in Fig. 14. We recover the expected trend of more massive subhaloes being more strongly clustered across finders. However, the values and shapes of the correlation functions can vary. Looking at large scales, beyond 1 to 10 Mpc, the agreement is generally good. Subfind and HBT-HERONS are the most consistent pair, but differences exist at the largest scales between the two highest V_{max} bins.

We note a small systematic shift in the values found at large scales between ROCKSTAR and HBT-HERONS. This is driven by the fact that a cut in subhaloes according to their V_{max} results in slightly different population selections. As discussed in §4.2.3, the bound mass of ROCKSTAR centrals is suppressed relative to all other subhalo finders. This means that selecting on ROCKSTAR's V_{max} selects subhaloes with larger average M_{200c} than those selected using the same V_{max} found by the three other subhalo finders. As more massive subhaloes are more strongly clustered, this selection biases the correlation function to be slightly larger at fixed V_{max} for ROCKSTAR relative to the other finders.

On scales smaller than ≈ 2 Mpc, where the one halo term contribution becomes important, the measured correlation functions differ significantly. The differences are due to how well the satellite systems are found by each subhalo finder. As such, most changes relative to HBT-HERONS are similar to those in the radial distribution functions. For example, the Subfind correlation functions are increasingly suppressed at small distances, regardless of the V_{max} bin.

Comparing the correlation functions in the hydrodynamical sim-

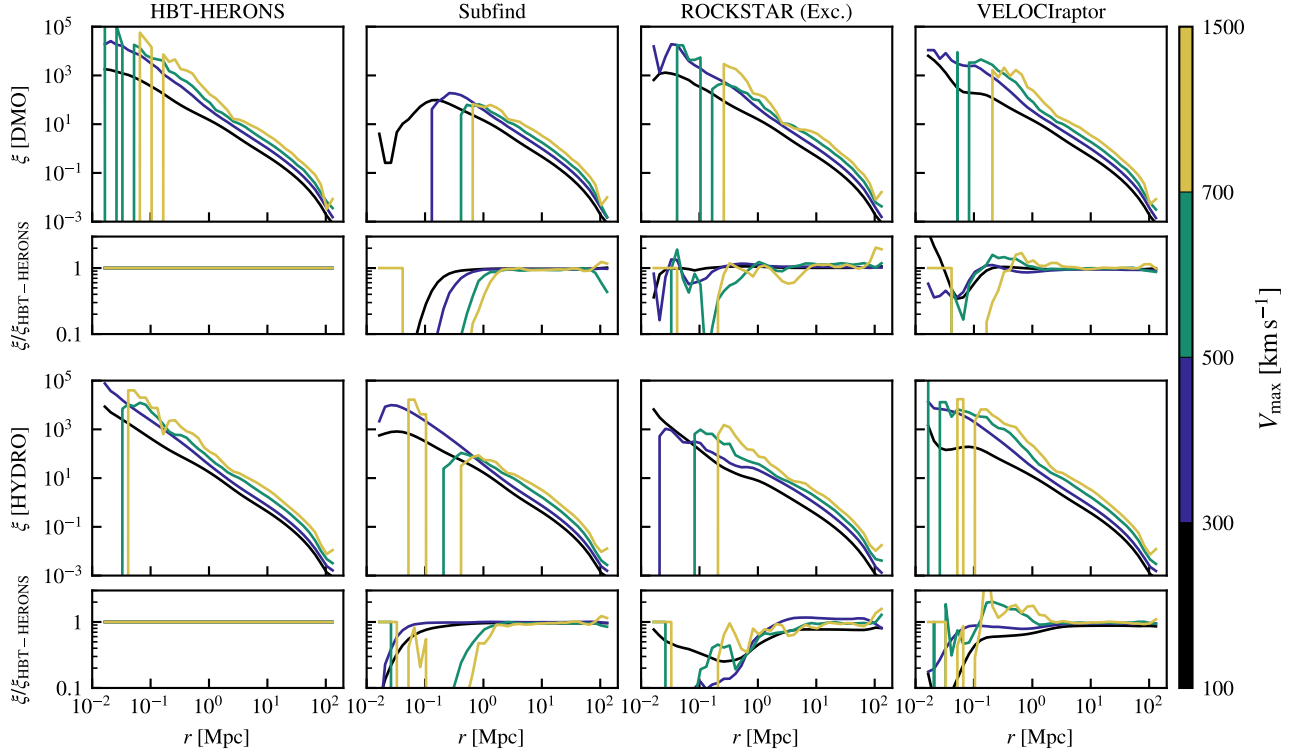


Figure 14. Auto-correlation function of subhaloes in the L1_m9 simulation, measured in different bins of V_{\max} (different colours). We select all subhaloes whose V_{\max} is within the limits of the corresponding bin, regardless of whether they classified as satellites or centrals. *Top panels:* the correlation functions found in the DMO version of the simulations. The secondary panel shows the ratio relative to the values found by HBT-HERONS. *Bottom panels:* Same as the top panels, but for the hydrodynamical version of the simulations. Note that for the purposes of this comparison, we modified ROCKSTAR to assign masses exclusively, which is the way mass is assigned by the other subhalo finders, but it is not ROCKSTAR’s default behaviour.

ulations, in the bottom panels of Fig. 14, we see that they change relative to DMO in a similar manner as the satellite radial distributions between DMO and hydro (see Fig. 11). Subhaloes are typically more strongly clustered at smaller scales in the hydro than in DMO simulations, which reflects the fact that more are present within the virial regions of their centrals at $z = 0$. As was argued before, this is likely due to a combination of longer survival times and easier identification of subhaloes thanks to their denser centres. For Subfind, this results in the clustering of the lowest V_{\max} subhaloes increasing at small scales relative to what is found in the DMO simulation. However, the two highest V_{\max} bins remain unchanged for Subfind, as the inclusion of hydro does not facilitate the identification of the most massive satellites.

The level of agreement between subhalo finders is different for the hydrodynamical simulations. ROCKSTAR and VELOCraptor become more discrepant relative to HBT-HERONS at small scales, which is caused by their worse performance in finding subhaloes once baryons are included (see §4.2). On the other hand, Subfind shows better agreement, as per the better identification of denser satellites within their associated haloes. However, the largest V_{\max} bin shows no improvement. As an increase in the resolution does not improve the identification of subhaloes with large ratios of satellite to host bound mass (Fig. 13), the population of merging high V_{\max} subhaloes will not be found. We therefore posit that the Subfind correlation functions in the highest V_{\max} bin will remain suppressed relative to HBT-HERONS even for simulations that reach higher resolutions and larger volumes.

5 CONCLUSIONS

Making inferences in the era of precision cosmology and large galaxy surveys requires quantifying how uncertain predictions are. One aspect that plays an important role is the identification of (sub)haloes and galaxies within simulations. The process of structure finding is non-trivial, as collapsed structures can be found in a variety of environments and evolutionary stages. In some instances, this results in the mischaracterisation of subhaloes and galaxies.

In this study, we have explored how the choice of subhalo finder influences basic summary statistics derived from a subset of the FLAMINGO DMO and hydrodynamical simulations (Schaye et al. 2023; Kugel et al. 2023). The FLAMINGO suite provides a good test bench to study how (sub)halo finding algorithms influence predictions relevant to large-scale surveys, as they provide a large statistical sample, include both DMO and hydrodynamical simulations spanning a large range of resolutions, and are tailored to reproduce observables relevant to such studies, e.g. cluster gas fractions and stellar mass functions.

For our analysis, we chose to compare four representative subhalo finding algorithms, all of which rely on running the Friends-of-Friends algorithm first. Each of the subhalo finders we use are representative of commonly used methods: configuration- (Subfind), phase- (ROCKSTAR & VELOCraptor) and history-space (HBT-HERONS). Subfind relies on identifying subhaloes based on finding spatial density peaks. VELOCraptor instead finds peaks in position and velocity space. ROCKSTAR is also based on phase-space finding, but runs a 6D FoF algorithm using the position and velocity of particles. HBT-HERONS uses the past evolution of subhaloes to tag

associated particles. The association is propagated forward in time to identify potential subhalo candidates, based on grouping particles that share a subhalo progenitor.

As each finder makes different assumptions and uses different methods to compute subhalo properties, we used an external tool (SOAP; McGibbon et al. in prep) to measure subhalo properties in a consistent manner. Additionally, we also implemented exclusive mass assignment in ROCKSTAR (i.e. a particle can only be bound to a single subhalo) so that it more closely resembles the manner in which the other three subhalo finders assign masses to subhaloes. To avoid trivial resolution effects, we only consider subhaloes with masses greater than 100 dark matter particles. Our main results can be summarised as follows:

(i) The computational cost and scalability of subhalo finders differs significantly. For the simulations we tested here, `Subfind` and `VELOCItaptor` took $\mathcal{O}(10^3)$ CPU-h to analyse the same output that took `HBT-HERONS` and `ROCKSTAR` only $\mathcal{O}(10)$ CPU-h. As an example, the `L1_m9` hydrodynamical `FLAMINGO` simulation took $\mathcal{O}(10^6)$ CPU-h to complete and contains 79 outputs. The cost of using `HBT-HERONS` and `ROCKSTAR` to find subhaloes across all outputs is negligible compared to the cost of running the simulation. In contrast, `Subfind` and `VELOCItaptor` require a comparable investment to running the simulation itself.

(ii) During the development of subhalo finders, the effects of adding baryons to simulations is often overlooked, because the algorithms are initially developed for and tested with dark-matter-only simulations. As such, key assumptions used in the finding process may not hold for hydrodynamical simulations. This generally results in poorer performance, with the number of catastrophic failures during the identification dramatically increasing. For `HBT+`, we addressed these issues by implementing a series of improvements in a new version named `HBT-HERONS`. These were primarily made with the objective of improving its subhalo finding and time-tracking performance in hydrodynamical simulations (§A1). However, the new additions also propagate to better tracking in dark-matter-only simulations (§A2, §A3, §A5, §A6, §A7). Additionally, a number of other longstanding issues, such as particle duplication in the catalogues (§A4) and inadequate particle partitioning, have also been solved.

(iii) All finders except `Subfind` and `HBT-HERONS` perform worse in hydrodynamical than in DMO runs. As a matter of fact, `Subfind` performs better for hydro than for DMO by virtue of more concentrated subhalo centres facilitating the identification of density peaks. However, for higher resolution simulations, e.g. with cold and dense gas clumps within the ISM or CGM, we expect `Subfind` to identify those clumps as separate subhaloes from the galaxy that hosts them, which would require additional processing to construct a galaxy catalogue.

(iv) Basic summary statistics that should ideally be relatively insensitive to the choice of subhalo finder, such as the M_{200c} mass functions, change by up to 10% (Fig. 3) and the differences are insensitive to resolution (Fig. 5). Only `HBT-HERONS` and `Subfind` agree within 1%. The discrepancies in the values we found are due to halo miscentering and differences in how central subhaloes are defined. Miscentering primarily affects `VELOCItaptor`, worsens for hydro, and causes 3%-level differences for well-resolved haloes. The definition of which subhalo is the central primarily affects `ROCKSTAR` and is the more problematic source of disagreement. This is because, beyond its induced 10%-level differences, it highlights that the current freedom in defining centrals causes systematic shifts. Although some authors may argue for or against a given definition, this effect should be accounted for when comparing with observations.

(v) Following from iv), an implicit choice made when running subhalo finders that assign a single central per FoF group (`HBT-HERONS`, `Subfind` and `VELOCItaptor`) is the FoF linking length. Given that there is no a priori correct choice when it comes to comparisons to observations, we explored how strongly the choice of linking length affects the resulting $z = 0$ M_{200c} mass functions of `HBT-HERONS`. We did this by varying the fiducial linking length of 0.2 to 0.16 and 0.25 times the mean interparticle separation. These linking lengths roughly correspond to a factor of two lower (0.25) and higher (0.16) overdensities relative to the commonly used choice. We found steeper and shallower mass functions for the shorter and longer linking lengths, respectively. This can change the predicted abundance of Milky Way-mass haloes by up to 6%, and the difference only drops below 1% for the most massive clusters of galaxies (Fig. 4).

(vi) The bound mass functions differ by larger amounts ($\approx 50\%$) than the M_{200c} mass functions (Fig. 6). `Subfind` assigns less mass to satellites than `HBT-HERONS`, which boosts the bound mass of the central subhaloes it finds. `VELOCItaptor` and `HBT-HERONS` agree well, although there are slightly more massive satellites in `VELOCItaptor`. This is likely due to the central definition, as `VELOCItaptor` does not require the most massive subhalo to be the central of a FoF group. `ROCKSTAR` satellites have a lot less bound mass than for the other finders, and the associated number densities also change more strongly with resolution (Fig. 7). Differences remain even when counting subhaloes as a function of V_{\max} instead of M_{bound} (Fig. 8), although it improves the agreement between `Subfind` and `HBT-HERONS`.

(vii) The normalisation and shape of the subhalo radial distributions are both sensitive to which subhalo finder is used. Close to R_{200c} , where the difficulties associated with analysing the dense core of haloes are less important, the number density of subhaloes, $n(r)$, can vary by as much as 20% between subhalo finders (Fig. 9). The shapes of the distribution within R_{200c} can also change dramatically, with 10% agreement for $n(r)/n(R_{200c})$ only reached beyond $0.1R_{200c}$ (Fig. 11). Out of the four subhalo finders we compare, `Subfind` struggles the most to find subhaloes near the central regions of haloes, as it exhibits a clear suppression in the number density of subhaloes at small radii regardless of M_{200c} . The problem with the identification of subhaloes by `Subfind` worsens as the mass of the satellite subhalo relative to its host increases, meaning that either the most massive satellite subhaloes are typically missing or their masses are severely suppressed relative to the values found in the other subhalo finders (Fig. 12). This occurs because the chosen central subhalo acquires most of the mass in the FoF group, leaving a subhalo with an otherwise comparable mass, severely depleted in particle content.

(viii) The inclusion of hydrodynamics increases the number of subhaloes near R_{200c} and steepens their number density profiles. This is likely driven by the cores of subhaloes becoming denser, both due to baryons being more concentrated than the DM and the increase in the central DM density in response to the baryons. As denser subhaloes are more resilient to disruption, more survive to $z = 0$. Additionally, the agreement between subhalo finders tends to improve, particularly for `Subfind`. This is because the more prominent density peaks are easier to identify against the backdrop of the halo they are embedded in.

(ix) Satellites are segregated by their mass relative to that of the host, with the more massive ones being more concentrated towards the centre of the host halo (Fig. 12). This is opposite to the trend found in previous studies based on `Subfind`, which claimed that more massive satellites are *less* concentrated towards the centre of their host. We think the interpretation offered in those studies suffered from

systematically biased subhalo catalogues. This major discrepancy across subhalo finders remains across resolution levels (Fig. 13). In other words, different subhalo finders converge to different answers.

(x) The auto-correlation functions of all subhaloes, when selected in bins of different V_{\max} , can differ at both large and small distances between different subhalo finders (Fig. 14). The disagreement between subhalo finders depends sensitively on the chosen V_{\max} bin, and worsens at small scales for larger values of V_{\max} , i.e. for subhaloes that should be well resolved. The primary difference in the two-point correlation function at large scales is a systematic offset between ROCKSTAR and the rest of the subhalo finders, caused by a different V_{\max} dependence on mass. Applying the same V_{\max} cut selects subhaloes of different average masses, and hence clustering strength. This reflects the fact that the V_{\max} of a subhalo is calculated using only the particles bound to it, so the unbinding procedure that each algorithm uses can influence its value. At small scales, the differences are driven by how well satellite systems can be recovered. As such, all subhalo finders under predict the correlation function relative to HBT-HERONS within ≈ 2 Mpc.

In short, (sub)halo finding is not a solved problem, and the choice of which algorithm to use needs to be made carefully. As it is unlikely, and probably undesirable, for the whole community to adopt a single approach to finding subhaloes and to use the same definitions – and none of the (sub)halo finding algorithms can be directly applied to observations – part of the uncertainty budget in making predictions should be devoted to the manner in which (sub)haloes are found. A related, but slightly different aspect, is how the properties of galaxies change across subhalo finders. As they are located in the centres of dark matter subhaloes, and the identification of a subhalo core is typically easier than the identification of its edge, the properties of galaxies may not differ as much as what we have discussed in this study.

Indeed, answering the question of which subhalo finder is the best to use is complicated. The difficulty arises primarily from the fact that there are no clear, definitive answers to the question of what the properties of any given subhalo population should be. Any realistic prediction to compare against is inevitably based on simulations, and hence on a series of choices of how the subhaloes were found and defined. As we have shown here, many differences exist depending on the chosen subhalo finder, so trying to ‘calibrate’ the performance of a subhalo finder to a reference solution is moot.

Nevertheless, some useful insights can still be gained. Imaging many haloes to identify whether any visually obvious subhaloes are missing from the catalogues reveals catastrophic failures (e.g. Fig. 2). The convergence of the properties of subhalo populations with increasing resolution, and whether the recovered trends are sensible, also provide a handle with which to identify better performing algorithms. However, this is always with the caveat that trends can often be explained by a variety of plausible mechanisms (e.g. the radial distribution of the most massive subhaloes) and that the finders seem to converge towards different answers as the resolution is increased. Lastly, an extremely powerful test is to examine the time evolution of the subhalo population, as failures difficult to identify at a fixed time can become evident when integrated over a Hubble time (e.g. Chandro-Gómez et al. 2025).

Based on the above methodology, we conclude that HBT-HERONS provides the most robust subhalo catalogues out of the four subhalo finders we have explored in this work. There are generally no visibly obvious subhaloes missing from its catalogues based on extensive imaging, and the trends and convergence appear sensible. For time-integrated tests, Chandro-Gómez et al. (2025) find that HBT-HERONS

drastically suppresses the number of unphysical results in the time evolution of subhalo populations compared to several combinations of alternative subhalo finders (VELOCItaptor and Subfind) and merger tree algorithms (D-Trees+DHALo, Jiang et al. 2014; and TreeFrog, Elahi et al. 2019b). As such, we make HBT-HERONS the default subhalo finder for the FLAMINGO simulations and make it publicly available.

ACKNOWLEDGEMENTS

This work used the DiRAC@Durham facility managed by the Institute for Computational Cosmology on behalf of the STFC DiRAC HPC Facility (www.dirac.ac.uk). The equipment was funded by BEIS capital funding via STFC capital grants ST/K00042X/1, ST/P002293/1, ST/R002371/1 and ST/S002502/1, Durham University and STFC operations grant ST/R000832/1. DiRAC is part of the National e-Infrastructure. VJFM acknowledges support by NWO through the Dark Universe Science Collaboration (OCENW.XL21.XL21.025). JXH acknowledges support from National Key R&D Program of China (2023YFA1607800, 2023YFA1607801), China Manned Space Project (No. CMS- CSST-2021-A03), and 111 project (No. B20019).

We thank Peter Behroozi, Pascal Elahi and Volker Springel for their useful comments and discussion during the preparation of this manuscript. This work has benefited from using `swiftsimio` (Borrow & Borrisov 2020), both to handle particle and (sub)halo data, and to image (sub)haloes. We thank Jeger Broxteman and Will McDonald for providing a suitable bird-related acronym.

DATA AVAILABILITY

The data used in this study can be made available upon reasonable request to the corresponding author. The HBT-HERONS algorithm (<https://github.com/SWIFTSIM/HBT-HERONS>) and SOAP package (<https://github.com/SWIFTSIM/SOAP>) are publicly available and can handle the data output of `Swift` simulations.

REFERENCES

- Abbott T. M. C., et al., 2022, *Phys. Rev. D*, **105**, 023520
- Angulo R. E., Lacey C. G., Baugh C. M., Frenk C. S., 2009, *MNRAS*, **399**, 983
- Aubert D., Pichon C., Colombi S., 2004, *MNRAS*, **352**, 376
- Bahé Y. M., et al., 2022, *MNRAS*, **516**, 167
- Behroozi P. S., Wechsler R. H., Wu H.-Y., 2013a, *ApJ*, **762**, 109
- Behroozi P. S., Wechsler R. H., Wu H.-Y., Busha M. T., Klypin A. A., Primack J. R., 2013b, *ApJ*, **763**, 18
- Behroozi P., et al., 2015, *MNRAS*, **454**, 3020
- Booth C. M., Schaye J., 2009, *MNRAS*, **398**, 53
- Borrow J., Borrisov A., 2020, *Journal of Open Source Software*, **5**, 2430
- Borrow J., Schaller M., Bower R. G., Schaye J., 2022, *MNRAS*, **511**, 2367
- Bryan G. L., Norman M. L., 1998, *ApJ*, **495**, 80
- Chaikin E., Schaye J., Schaller M., Bahé Y. M., Nobels F. S. J., Ploekinger S., 2022, *MNRAS*, **514**, 249
- Chaikin E., Schaye J., Schaller M., Benítez-Llambay A., Nobels F. S. J., Ploekinger S., 2023, *MNRAS*, **523**, 3709
- Chandro-Gómez Á., et al., 2025, *arXiv e-prints*, p. [arXiv:2501.07677](https://arxiv.org/abs/2501.07677)
- Dalla Vecchia C., Schaye J., 2008, *MNRAS*, **387**, 1431
- De Lucia G., Kauffmann G., Springel V., White S. D. M., Lanzoni B., Stoehr F., Tormen G., Yoshida N., 2004, *MNRAS*, **348**, 333
- Diemer B., Behroozi P., Mansfield P., 2024, *MNRAS*, **533**, 3811
- Driver S. P., et al., 2022, *MNRAS*, **513**, 439

- Drlica-Wagner A., et al., 2019, *arXiv e-prints*, p. [arXiv:1902.01055](https://arxiv.org/abs/1902.01055)
- Efstathiou G., Sutherland W. J., Maddox S. J., 1990, *Nature*, **348**, 705
- Elahi P. J., Thacker R. J., Widrow L. M., 2011, *MNRAS*, **418**, 320
- Elahi P. J., Cañas R., Poulton R. J. J., Tobar R. J., Willis J. S., Lagos C. d. P., Power C., Robotham A. S. G., 2019a, *Publ. Astron. Soc. Australia*, **36**, e021
- Elahi P. J., Poulton R. J. J., Tobar R. J., Cañas R., Lagos C. d. P., Power C., Robotham A. S. G., 2019b, *Publ. Astron. Soc. Australia*, **36**, e028
- Elbers W., Frenk C. S., Jenkins A., Li B., Pascoli S., 2021, *MNRAS*, **507**, 2614
- Elbers W., Frenk C. S., Jenkins A., Li B., Pascoli S., 2022, *MNRAS*, **516**, 3821
- Euclid Collaboration et al., 2023, *A&A*, **671**, A100
- Euclid Collaboration et al., 2024a, *arXiv e-prints*, p. [arXiv:2405.13491](https://arxiv.org/abs/2405.13491)
- Euclid Collaboration et al., 2024b, *arXiv e-prints*, p. [arXiv:2405.13495](https://arxiv.org/abs/2405.13495)
- García R., Rozo E., 2019, *MNRAS*, **489**, 4170
- Garrison-Kimmel S., et al., 2017, *MNRAS*, **471**, 1709
- Genel S., Genzel R., Bouché N., Naab T., Sternberg A., 2009, *ApJ*, **701**, 2002
- Gill S. P. D., Knebe A., Gibson B. K., 2004, *MNRAS*, **351**, 399
- Giocoli C., Tormen G., Sheth R. K., van den Bosch F. C., 2010, *MNRAS*, **404**, 502
- Gómez J. S., Padilla N. D., Helly J. C., Lacey C. G., Baugh C. M., Lagos C. D. P., 2022, *MNRAS*, **510**, 5500
- Griffen B. F., Ji A. P., Dooley G. A., Gómez F. A., Vogelsberger M., O’Shea B. W., Frebel A., 2016, *ApJ*, **818**, 10
- Guo Q., White S., 2014, *MNRAS*, **437**, 3228
- Hagar R., Pearce F. R., Gray M. E., Knebe A., Yepes G., 2021, *MNRAS*, **502**, 1191
- Hahn O., Martizzi D., Wu H.-Y., Evrard A. E., Teysier R., Wechsler R. H., 2017, *MNRAS*, **470**, 166
- Hahn O., Rampf C., Uhlemann C., 2021, *MNRAS*, **503**, 426
- Han J., Jing Y. P., Wang H., Wang W., 2012, *MNRAS*, **427**, 2437
- Han J., Cole S., Frenk C. S., Benítez-Llambay A., Helly J., 2018, *MNRAS*, **474**, 604
- Huško F., Lacey C. G., Schaye J., Schaller M., Nobels F. S. J., 2022, *MNRAS*, **516**, 3750
- Jiang L., Helly J. C., Cole S., Frenk C. S., 2014, *MNRAS*, **440**, 2115
- Jung M., et al., 2024, *ApJ*, **964**, 123
- Kitzbichler M. G., White S. D. M., 2008, *MNRAS*, **391**, 1489
- Klypin A., Gottlöber S., Kravtsov A. V., Khokhlov A. M., 1999, *ApJ*, **516**, 530
- Knebe A., et al., 2011, *MNRAS*, **415**, 2293
- Knollmann S. R., Knebe A., 2009, *ApJS*, **182**, 608
- Kugel R., et al., 2023, *MNRAS*, **526**, 6103
- Kugel R., Schaye J., Schaller M., Moreno V. J. F., McGibbon R. J., 2025, *MNRAS*,
- Mansfield P., Darragh-Ford E., Wang Y., Nadler E. O., Diemer B., Wechsler R. H., 2024, *ApJ*, **970**, 178
- More S., Kravtsov A. V., Dalal N., Gottlöber S., 2011, *ApJS*, **195**, 4
- Necib L., Lisanti M., Garrison-Kimmel S., Wetzel A., Sanderson R., Hopkins P. F., Faucher-Giguère C.-A., Kereš D., 2019, *ApJ*, **883**, 27
- Onions J., et al., 2012, *MNRAS*, **423**, 1200
- Peñarrubia J., Benson A. J., Walker M. G., Gilmore G., McConnachie A. W., Mayer L., 2010, *MNRAS*, **406**, 1290
- Pizzati E., et al., 2024, *arXiv e-prints*, p. [arXiv:2403.12140](https://arxiv.org/abs/2403.12140)
- Ploekinger S., Schaye J., 2020, *MNRAS*, **497**, 4857
- Press W. H., Davis M., 1982, *ApJ*, **259**, 449
- Pujol A., et al., 2014, *MNRAS*, **438**, 3205
- Pujol A., et al., 2017, *MNRAS*, **469**, 749
- Riggs S. D., Loveday J., Thomas P. A., Pillepich A., Nelson D., Holwerda B. W., 2022, *MNRAS*, **514**, 4676
- Samuel J., et al., 2020, *MNRAS*, **491**, 1471
- Sawala T., Pihajoki P., Johansson P. H., Frenk C. S., Navarro J. F., Oman K. A., White S. D. M., 2017, *MNRAS*, **467**, 4383
- Schaller M., et al., 2024, *MNRAS*, **530**, 2378
- Schaye J., Dalla Vecchia C., 2008, *MNRAS*, **383**, 1210
- Schaye J., et al., 2015, *MNRAS*, **446**, 521
- Schaye J., et al., 2023, *MNRAS*, **526**, 4978
- Sharma S., Steinmetz M., 2006, *MNRAS*, **373**, 1293
- Sinha M., Garrison L. H., 2020, *MNRAS*, **491**, 3022
- Springel V., White S. D. M., Tormen G., Kauffmann G., 2001, *MNRAS*, **328**, 726
- Springel V., et al., 2005, *Nature*, **435**, 629
- Springel V., Pakmor R., Zier O., Reinecke M., 2021, *MNRAS*, **506**, 2871
- Villaescusa-Navarro F., et al., 2023, *The Astrophysical Journal Supplement Series*, **265**, 54
- Vogelsberger M., et al., 2009, *MNRAS*, **395**, 797
- Wang J., Frenk C. S., Navarro J. F., Gao L., Sawala T., 2012, *MNRAS*, **424**, 2715
- White S. D. M., Frenk C. S., Davis M., 1983, *ApJ*, **274**, L1
- Wiersma R. P. C., Schaye J., Theuns T., Dalla Vecchia C., Tornatore L., 2009, *MNRAS*, **399**, 574

APPENDIX A: DIFFERENCES BETWEEN HBT-HERONS AND HBT+

As mentioned in §3, several improvements were made to the HBT+ algorithm, resulting in a version of the subhalo finder named HBT-HERONS. These changes primarily target the tracking of subhaloes, and hence improve the capabilities of HBT+ in both DMO and hydrodynamical simulations. However, some changes were specifically tailored for hydrodynamical simulations (§A1). In this Appendix, we explain in detail what all the changes are and their motivation.

An important step that we refer to in several occasions below is particle ‘masking’. This is done internally within HBT+ and HBT-HERONS before analysing any given FoF group, and the aim is to ensure that no particles are shared across subhaloes that belong to the same hierarchical branch. The process proceeds as follows. First, the IDs of particles that are associated to subhaloes without any children subhaloes are logged in a list. Next, their parent subhaloes check whether any of the IDs of their respective particles are already in the list. The particles with a match are removed from the source of the parent subhalo, i.e. the particles are masked. The parent subhalo retains the particles without any matches, and adds their IDs to the list. This process is repeated for each subhalo going up the hierarchy until the central subhalo is reached. The end result is that the particle distribution of each subhalo has the particles associated to other subhaloes ‘masked’ out. As masking only occurs between within a given hierarchical branch, there is no masking across FoF groups.

A1 Collisionless, time-persistent particle tracers

The original HBT+ algorithm relies on identifying the most bound particle of each subhalo as the tracer of its location. The FoF group membership of the tracer particle is subsequently used to determine which FoF group hosts a given subhalo. As this is used internally to determine the hierarchical relations of subhaloes within a FoF group, the tracer particle plays an important role. Additionally, the tracer particle is also used to identify the position and velocity of orphaned subhaloes. HBT+ does not take into account the particle type of the tracer, meaning it can choose a gas or black hole particle if these are the most bound ones. If the chosen tracer particle is a gas particle then it can be ejected from the halo by feedback, and if the tracer is a black hole particle, then it can merge with another black hole and cease to exist.

If the tracer is indeed blown out from a FoF group, the subhalo will be deemed hostless, even if the majority of its constituent particles remain part of a FoF group. The inappropriate choice of particle tracer has important ramifications, as it leads to the sudden

loss of well-resolved substructure. We illustrate how this happens in the diagram shown in Fig. A1. In this example, we start with two subhaloes in the same FoF group, with Track 0 being the central. The most bound particle of each subhalo is located at its centre, but crucially, the tracer of Track 0 is a gas particle.

Between outputs N and $N+1$, the galaxy experiences a gas outflow, e.g. resulting from AGN activity. Consequently, the gas tracer particle is ejected from the FoF group. In output $N+1$, the FoF group has no central, as the algorithm has identified Track 0 as hostless. Therefore, the most massive satellite becomes its central, i.e. Track 1. In doing so, the particles that belonged to Track 0 and 1 get grouped together. As HBT+ bases its subhalo identification on the past membership of particles, it will be unable to identify the satellite subhalo as a separate entity from the central throughout the remainder of the simulation.

Another problem resulting from this example is that, since HBT+ allows the existence of hostless subhaloes, Track 0 retains its previously associated particles. This means that Tracks 0 and 1 share large numbers of bound particles in output $N+1$. Their most bound particles will thus be located close in phase-space. Despite the significant overlap between both subhaloes, no merger condition is triggered because they are formally not in the same FoF group. In output $N+2$, if no other blowouts occur, both subhaloes will be located in the same FoF group. However, HBT+ assigns particles within a FoF group to subhaloes in an exclusive manner by applying a mask. The significant overlap in particle content between subhaloes means that one of the two subhaloes is masked out of existence, leading to the sudden loss of a subhalo.

The chain of events described above can happen several times to a subhalo throughout a simulation, potentially affecting more than one satellite. Since the occurrence of the problem only requires the misidentification of the FoF group based on a single particle, it can happen to subhaloes regardless of how well resolved they are. To address this issue, HBT-HERONS can constrain which particle type is allowed to be a tracer of a subhalo. Ideal particle tracers are collisionless and time persistent. In the FLAMINGO simulations, only star and dark matter particles types satisfy these two requirements simultaneously. To reflect this, HBT-HERONS defaults to only allowing star or dark matter particles to be subhalo particle tracers.

Our preference towards using time-persistent and collisionless particles as tracers is reflected in other HBT-HERONS routines relying on a subset of the most bound particles of a subhalo. For example, orphans are constrained to use the most bound star or dark matter particle when they were last resolved. However, in HBT+, they could have been assigned to a gas or black hole particle. This change solves issues stemming from using gas and black hole tracers, since they can disappear from the simulation, leading to the loss of the orphan.

A2 Weighted host finding

Once a tracer particle has been assigned to a subhalo, its FoF membership is used at the next output time to identify which FoF group hosts the subhalo it is associated to. In HBT+ this approach thus relies on a single particle, and is hence prone to discreteness noise. For host finding, this noise primarily manifests itself as the tracer straying away from the core of a subhalo. This produces a clear mismatch between the FoF group assigned to a subhalo, and the actual FoF group where the majority of the core particles of the subhalo end up.

Similar to the issue discussed in §A1, the incorrect assignment of the FoF group of a subhalo has important ramifications. We explain the issues that arise as a consequence with the example shown in Fig. A2. In output N , we have a single central subhalo with TrackId 0. At the next output, its tracer has strayed away from the FoF group

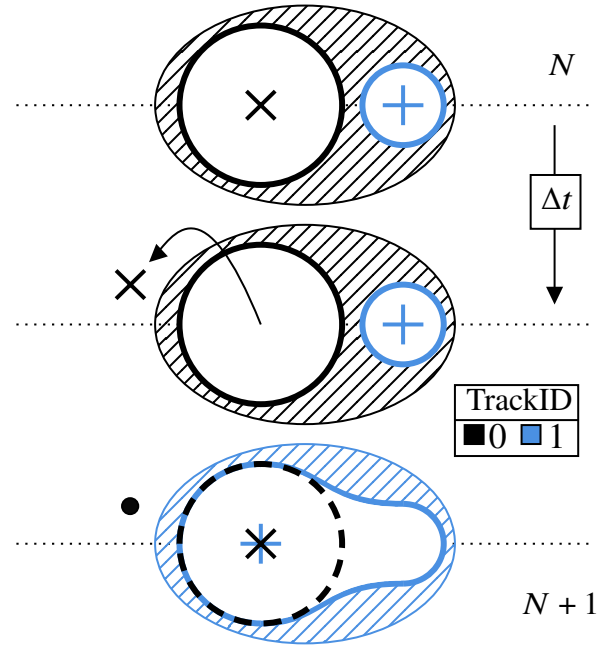


Figure A1. Schematic representation of how using gas as particle tracers of subhaloes may lead to the loss of satellites in HBT+. Each column shows the time evolution of a unique subhalo, whose bound component at a given time is represented by a circle. Different colours correspond to different evolutionary branches, whose TrackIDs are given by the legend. The shaded ellipses are FoF groups, coloured as their corresponding central subhalo. The crosses and pluses represent the centre of each subhalo, which is the position of its most bound tracer particle. The filled circle represents an individual particle. Initially, Tracks 0 and 1 are contained in the same group. The gas tracer of the central subhalo, Track 0, is blown out of the FoF group. This makes HBT+ reassign Track 1 as the new central, as Track 0 is now a hostless subgroup. This mixes the particles of the two existing subhaloes together, making HBT+ unable to identify the actual subhalo that Track 1 was meant to track. Since TrackId 0 retains its previous particles, the two subhaloes now share a large number of particles. Thus, in output $N+1$, both subhaloes are likely to have the same position in phase-space, but no merging checks are applied as HBT+ incorrectly thinks they are in separate FoF groups.

and the subhalo is deemed hostless. This is in contrast to the majority of its associated particles, as they remain within a FoF group. In this example, since said FoF group has no associated central, a new subhalo is spawned with TrackId 1. The subhaloes now share a large fraction of their particles, as masking is not done across FoF groups, and will likely end up with the same tracer in output $N+1$. Eventually, if the tracer of TrackId 0 is found in the same FoF as TrackId 1 in output $N+2$, one of the two will be masked.

Contrary to the problem discussed in §A1, this issue only arises for subhaloes that are poorly sampled by particles. This is because the spatial extent of FoF groups with $\mathcal{O}(10^2)$ particles is much smaller than groups with many more particles. Consequently, a particle that is near the centre of the FoF group can more easily make it beyond its outskirts in the time difference between two consecutive time outputs. As the number density of subhaloes increases with decreasing subhalo mass, this issue results in many short-lived spuriously-created subhaloes. We note that the subhaloes prone to experience this appear to be more elongated than subhaloes of similar mass that do not exhibit the same issue. Presumably, this facilitates the tracer particle straying away from the FoF group along the minor axis of its particle distribution.

In order to not rely on a single particle, the host finding in

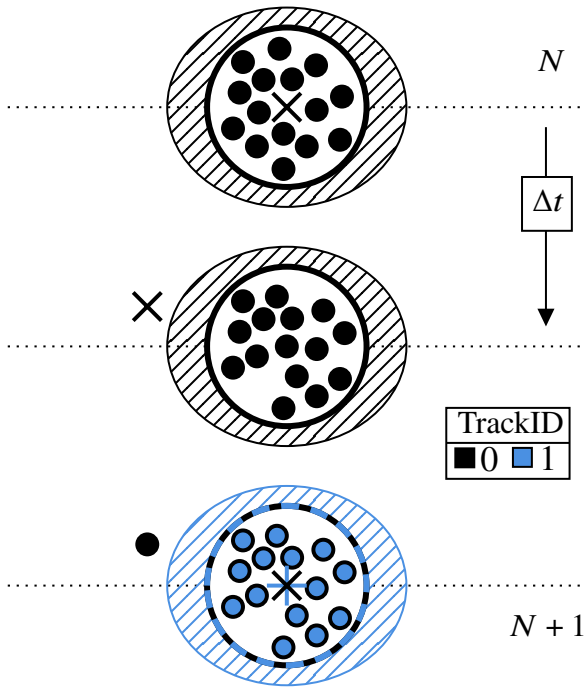


Figure A2. Schematic representation (as in Fig. A1) of how noise in the particle distribution may lead to misidentification of the FoF group hosting a central subhalo in HBT+. Initially, there is a single subgroup (Track 0). Subsequently, its tracer particle is not part of any FoF group, and hence HBT+ makes Track 0 hostless. This is in contrast to the bulk of its particles, which remain within the FoF group. Since the FoF group has no subhalo associated to it, a new subhalo (Track 1) is created. Similar to the example shown in Fig. A1, the two subhaloes share a large number of particles.

HBT-HERONS is done through a weighted estimate of the $N_{\text{host-finding}}$ (10) most bound collisionless tracers. The weight assigned to each particle, w_i , reflects their boundness ranking in the previous output, r_i . The functional form is given by equation (4) (e.g. Springel et al. 2021).

This improves the tracing of subhaloes in hydrodynamical and DMO simulations, as the host is not determined by a single particle. Given the reliance of the algorithm on using more than one particle tracers, we require at least $N_{\text{tracer}}^{\text{min}}$ particles of the accepted tracer type (equal to $N_{\text{host-finding}}$ by default) to be present in any subhalo for it to be deemed resolved. In other words, a resolved subhalo requires at least $N_{\text{bound}}^{\text{min}}$ total bound particles and $N_{\text{tracer}}^{\text{min}}$ bound particles that are valid tracer particle types.

We note that there are still subhaloes deemed as hostless even with this improved host finding method. Their existence is not necessarily unphysical, as it simply reflects the fact that linking particles close to the resolution limit of the simulation is noisy. In other words, a FoF group with a self-bound subhalo may lose one particle and dip below the threshold to be found as a FoF group. This makes the subhalo hostless, even though not much might have changed in terms of its self-boundness.

A3 Phase-space calculations

An important step in HBT+ that is not generally required for other subhalo finders is to check whether resolved subhaloes overlap in position and velocity space. The reason is that HBT+ is able to find two separate resolved subhaloes even if they have coalesced following a major merger. This is not a problem for alternative algorithms, like

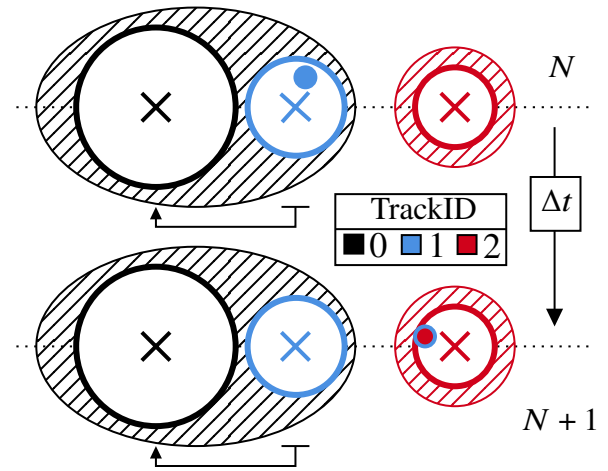


Figure A3. Schematic representation (as in Fig. A1) of how a stray particle originally associated to a satellite subhalo in a different FoF can lead to its duplication in HBT+. Initially, the particle is bound and associated to Track 1. In the next output, the particle is found in the FoF group whose central is Track 2. This means that the source subgroup of Track 2 acquires the particle, and it is found to be bound. However, the source subhalo of Track 1 still contains the particle in question, which can also be found to be bound. Hence, the particle is bound to two different subhaloes and appears duplicated in the catalogues. HBT-HERONS constrains particles to be part of the same FoF group as the Track they are associated to, if the particle are found in any FoF group. For this example, Track 1 would lose the particle since they are no longer located in the same FoF group.

those relying on density peaks, as they stop being able to distinguish coalescing subhaloes long before the merger is complete. Failing to manually merge overlapping subhaloes in HBT+ would lead to a spurious increase in the satellite number density at extremely close distances from the centre of haloes.

Computing the offset in phase-space between two pairs of subhaloes requires assigning a location to each (equation 6). In HBT+, the higher mass subhalo of a given hierarchical pair uses the centre of mass position and velocity of its 10 most bound tracers. The lower mass subhalo only uses its most bound particle tracer to locate its centre in position and velocity space.

However, using only one particle to estimate the phase-space location of subhaloes can be prone to noise. Therefore, HBT-HERONS estimates the phase-space position of both subhaloes in a hierarchical pair using the same number of particles (10 most bound tracers by default) as the most massive of the pair. Only when the least massive subhalo of the pair is an orphan, i.e. it only has one tracer particle, do we revert to using one particle to estimate its position and velocity.

A4 Exclusive particle membership

An inconsistency present in HBT+ is that particles can be shared among subhaloes, and hence appear duplicated in the catalogues. This is clearly unintended behaviour, as it would occur even when mass was supposed to be assigned to subhaloes in an exclusive manner. There are three main reasons that would result in particle duplication, which are facilitated by the fact that there is no particle masking for exclusive mass assignment across separate FoF groups. We explain each below, with an accompanying diagram when applicable.

The first reason is that particles associated to a satellite subhalo can end up in a different FoF group than its host. We illustrate how this can happen in Fig. A3. The particle retains its association to the

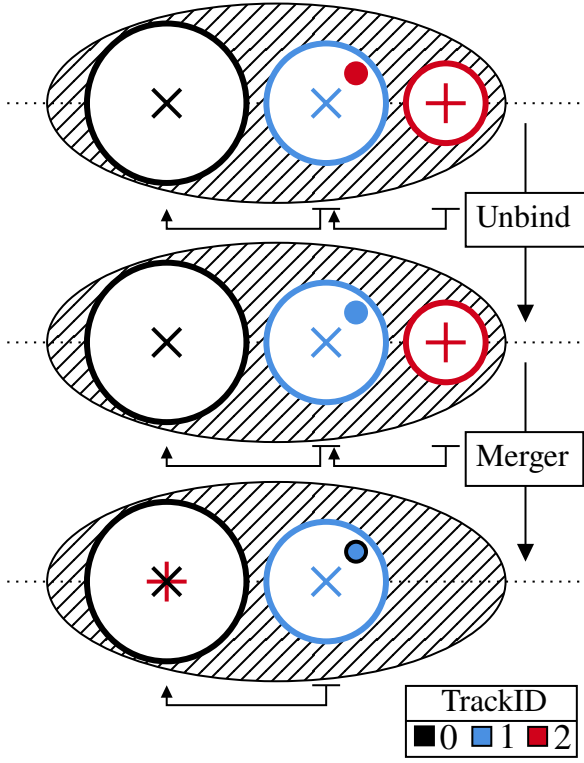


Figure A4. Schematic representation (as in Fig. A1) of how the previous way of dealing with subhalo mergers can lead to duplicate particles in HBT+. The rows represent distinct steps done when analysing the subhaloes in a FoF group during a single time output. The particle is originally associated to the source subhalo of Track 2, but is not bound to it. It is instead bound to Track 1, but it remains in the source of Track 2. After analysing all Tracks in the FoF, merging checks happen, and Track 2 merges with Track 0. All the particles previously associated to Track 2 are now part of the source subhalo of Track 0. A new unbinding iteration is triggered for Track 0, to account for the newly accreted mass. The original particle is now also bound to Track 0, and the duplication occurs because it is bound to Tracks 0 and 1. HBT-HERONS only allows the subhalo that accretes particles during a merger to acquire the bound particles of the merged subhalo. For this example, the particle will only be bound to Track 1.

satellite that it was originally bound to, reflecting its past history. However, the central in the FoF group that the particle is currently in also adds it to its source subhalo. Since no particle masking occurs across FoF groups, the particle can be found to be bound to both subhaloes. HBT-HERONS addresses this by required that, if a particle is found in a FoF group, any previous association to subhaloes in a different FoF group are removed.

The second cause is two related choices in how the re-unbinding following a subhalo merger is done. HBT+ only triggers the re-unbinding after analysing every subhalo in a given FoF group. Additionally, the unbinding is only done for the subhaloes that accreted another subhalo through a merger. As mergers can happen between subhaloes of different depths, this can lead to duplication of particles. We show an example of how this can happen in Fig. A4. This issue is fixed in HBT-HERONS by doing the merging checks immediately after the unbinding of a given subhalo, and only passing the particles bound to the now-merged subhalo onto the subhalo it merged with.

The final cause is the specific implementation of how unbound particles are internally passed between child-parent subhalo pairs. Specifically, if a particle is not bound to a subhalo, it is passed onto its parent subhalo to check if it is bound to it instead. Internally, this is

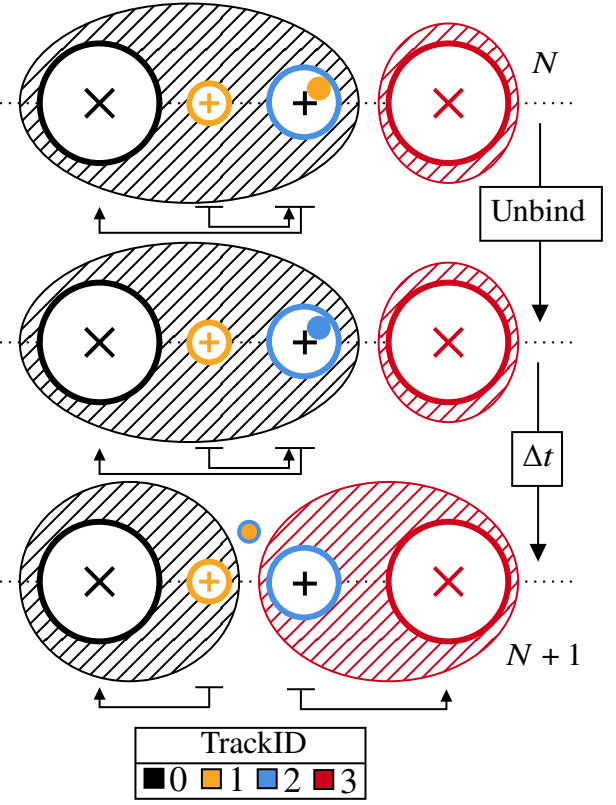


Figure A5. Schematic representation (as in Fig. A1) of how the incorrect assignment of particles to more than one source subhalo can lead to particle duplication in HBT+. The filled circle corresponds to an individual particle that is originally associated to Track 1. After unbinding is done, the particle is now bound to Track 2. Similar to the example of Fig. A4, this means the particle now belongs to the source subhalo of both Track 1 and Track 2. In the next output, Track 1 and 2 are satellites in different FoF groups. As there is no particle masking across different FoF groups, the particle can be found as bound to both Tracks and hence be duplicated. This duplication process only occurs if the particle in question is not part of a FoF group, as the fix for the Fig. A3 would otherwise be able to handle it. HBT-HERONS constrains particles to belong to a single source subhalo after unbinding every subhalo in the FoF group. The particles are preferentially assigned to original source subhalo from which they originated. For this example, the particle will only be bound to Track 1, as it is the subhalo the particle was originally associated with.

equivalent to adding the particle to the source subhalo of the parent. However, the particle may still remain in the source of its original subhalo if it was not trimmed from it (see §3.2.4). This is not an issue if both subhaloes remain in the same FoF group in the next output, as inter-FoF particle masking will remove the duplicate particle from the relevant source. However, if the subhaloes are found in different FoFs, the particle can be bound to both, as shown in Fig. A5. Note that an additional condition for this to occur is that the particle is not found in a FoF group. Otherwise, the fix shown for case Fig. A3 would handle this case. To remedy this problem, HBT-HERONS applies a mask on the source of subhaloes after the analysis of a whole FoF group is done. The masking preferentially gives particles to more deeply nested subhaloes, to reflect the fact that those particles always originate from deeper subhaloes.

A5 Orphan tracking and mass assignment

Orphan subhaloes are subhaloes that were self-bound in the past, but whose particles have been stripped causing the subhaloes to fall below the resolution limit of the simulation. In HBT+ and HBT-HERONS, their position and velocities are subsequently tracked using the most bound particle tracer when they were last resolved. In HBT+, the orphan tracer particles are explicitly associated to orphan subhaloes. This means that, as mass is assigned in an exclusive manner, subhaloes with many particles associated to orphans would have less mass.

Another closely related problem is that a particle already associated with an orphan subhalo could well be the most bound particle of a resolved subhalo. Thus, in HBT+, the resolved subhalo would be unable to acquire its ‘true’ most bound particle and would hence be traced by an incorrect particle if it subsequently became an orphan. As these situations can happen several times over the course of a simulation, the most bound core of resolved subhaloes could potentially become dominated by orphan subhaloes and not be explicitly bound to resolved subhaloes.

In HBT-HERONS, particle tracers are no longer explicitly assigned to orphan subhaloes, relying instead on locating the tracer particle properties based on ID matching. This means that orphan subhaloes can be identified, whilst their bound mass can be correctly assigned to a resolved subhalo. This change also allows for the possibility of more than one orphan being assigned to a single tracer particle.

A6 Descendants of disrupted subhaloes

In HBT+, resolved subhaloes can cease to exist in two different ways: disruption and merging. Disruption occurs when the number of bound particles drops below a given threshold, which is set by default to $N_{\text{bound}}^{\text{min}} = 20$. Mergers happen between subhaloes that are identified as self-bound but overlap sufficiently in phase space. Only a minority of subhaloes undergo actual mergers while still being resolved. Most fall below the resolution limit before sinking to the centre of their host subhalo.

HBT+ only provides information about the descendants of resolved mergers, i.e. which subhalo overlapped in phase space with the merged one. Thus, the merger trees built by HBT+ do not incorporate information about the descendants of (unresolved) mergers resulting from subhalo disruption. HBT-HERONS provides the required information to build complete merger trees, by outputting descendant information for both merged and disrupted subhaloes. To assign a descendant subhalo to each disrupted subhalo (‘DescendantTrackId’), HBT-HERONS uses the $N_{\text{descendant}}$ (10 by default) most bound particles from the previous output of the now-disrupted subhalo. The subhalo that contains the majority of this set of $N_{\text{descendant}}$ particles is the descendant of the disrupted subhalo.

A7 Refinement of the centres of subhaloes

HBT+ randomly subsamples the particle distribution of subhaloes whose source contains more than $N_{\text{subsample}}$ particles (1000 by default) to compute the gravitational potential during unbinding. If the source subhalo contains more particles than this threshold, it randomly selects $N_{\text{subsample}}$ particles, and if it contains fewer, it uses all particles for potential estimates. The subsampling is done with the aim of speeding up the unbinding iterations, which are often one of the most expensive calculations within halo finding. Although this approximate method works well to identify which particles are bound, their relative binding energies are affected by the choice of subsampled particles. Thus, this can influence the estimated subhalo

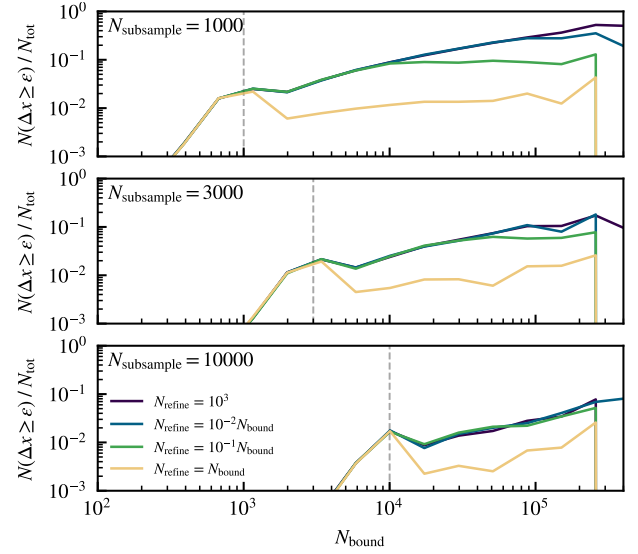


Figure A6. The fraction of resolved subhaloes whose centre is offset from its counterpart in a different HBT-HERONS run by more than the softening length of the DMO L1_m9 simulation ($\epsilon = 5.7$ kpc). Each panel corresponds to using a different choice for the number of particles used to subsample the potential calculation when unbinding subhaloes. The line colour reflects how many particles are used to refine the centre of the subhalo, with a constant value of 10^3 being the choice used in HBT+.

centre from run to run, as it is defined based on its most bound particle.

To address this, HBT+ does a ‘centre refinement’ after completing the unbinding of a subhalo. This consists of computing the self-binding energy of the $N_{\text{refine}} = N_{\text{subsample}}$ most bound particles identified during the subsampled unbinding. The most bound particle of that subset is then the centre of the subhalo. This approach works well, except if the subhalo in question has $N_{\text{bound}} \gg N_{\text{refine}}$. This is because the chosen subset becomes a very small fraction of the overall number of bound particles, and randomness in the subsampled unbinding step becomes increasingly important. For example, if $N_{\text{bound}} = 10^{10}$, one must correctly identify the centre based on 10^{-7} of bound particles. In practice, this is almost impossible to do, and hence the centre is likely significantly offset from the true centre found using all particles during unbinding.

In order to reduce the effect of subsampling on the identification of subhalo centres, HBT-HERONS scales N_{refine} with N_{bound} whenever $N_{\text{bound}} > N_{\text{subsample}}$:

$$N_{\text{refine}} = 0.1 N_{\text{bound}}. \quad (\text{A1})$$

The proportionality factor was chosen based on the tests shown in Fig. A6. To perform these tests, we first ran HBT-HERONS using the HBT+ configuration until the second to last snapshot of the DMO L1_m9 simulation. We then re-ran HBT-HERONS on the last snapshot using different choices for $N_{\text{subsample}}$ and N_{refine} , and independently run each combination 5 times to quantify the run-to-run scatter. We then compared the offset between pairs of matched subhaloes across runs that use the same configuration.

For the parameter choices of HBT+ ($N_{\text{subsample}} = N_{\text{refine}} = 10^3$), the fraction of matched counterparts whose centre deviates by more than the gravitational softening length is 0.53. For the same value of $N_{\text{subsample}}$, making N_{refine} scale as in equation A1 reduces this fraction to 0.13. This scaling is accompanied by an increased computational cost, although it amounts to an average of only +2% for

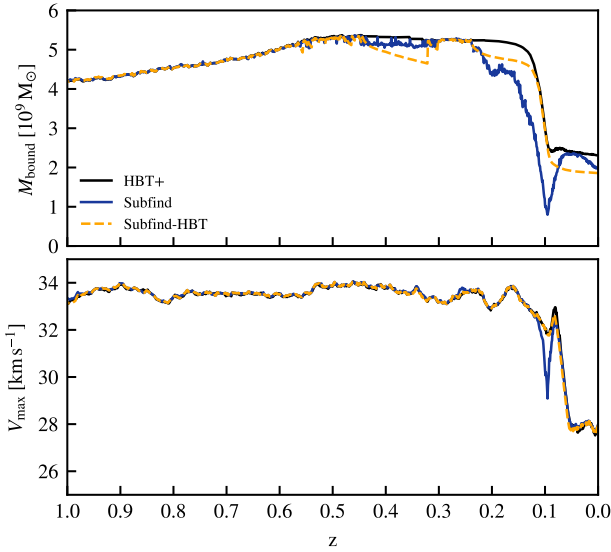


Figure B1. The bound mass (top panel) and V_{\max} (bottom panel) time evolution of a $z = 0$ subhalo, measured by HBT+ (solid black), Subfind (solid blue) and Subfind-HBT (dashed orange).

this simulation. In contrast, doing the unbinding without any subsampling of the particles takes +54% extra. We note that the additional cost of the better refinement will depend on the number of objects with $N_{\text{bound}} \geq N_{\text{subsample}}$, i.e. it will depend on the resolution and box size.

Exploring alternative choices for the scaling of N_{refine} and $N_{\text{subsample}}$, we identify several trends. There is a sharp decrease in the fraction of offset subhaloes whose particle number is below $N_{\text{subsample}}$, indicating the approximate threshold where particle subsampling no longer takes place. However, there is no sudden truncation, as the subsampling is based on the number of particles associated to the subhalo, rather than its bound particles. Thus, even if a subhalo has $N_{\text{bound}} = 500$, it would have been subject to subsampling if its source (see §3.2.4) had more than 10^3 particles. Additionally, for a fixed value/scaling of N_{refine} , the spatial offsets are smaller if $N_{\text{subsample}}$ increases. This is because the (approximate) relative binding energies are estimated more accurately, so picking the correct most bound particle subset is less prone to run-to-run randomness. Indeed, doing no subsampling would mean no centre refinement would be required. Lastly, the runs where we set $N_{\text{refine}} = N_{\text{bound}}$ highlight the effect of identifying different sets of bound particles due to potential subsampling. In other words, if a subhalo with the same set of bound particles would have its centre refined, the same centre would always be chosen for $N_{\text{refine}} = N_{\text{bound}}$. The fact that there is still a non-zero offset indicates that the same subhalo in different runs has a similar yet-different set of particles bound to it.

APPENDIX B: DIFFERENCES BETWEEN HBT+ AND SUBFIND-HBT

The similar names of the HBT+ and Subfind-HBT subhalo finders may suggest that they are the same algorithm. Although both rely on history-space, the details of how this approach is implemented differs. This can lead to small, yet systematic differences when comparing the properties and evolution of subhaloes matched between catalogues.

As such, they should be thought of as two independent halo finding algorithms, rather than HBT+ running on-the-fly within GADGET-4.

To illustrate the differences, we show how the bound mass of a $z = 0$ satellite subhalo evolves with time according to HBT+ and Subfind-HBT in Fig B1. Note that this example subhalo was taken from a GADGET-4 zoom-in dark-matter-only simulation of a $M_{200c} \approx 10^{12} M_{\odot}$ halo. The particle mass is $m_{\text{DM}} = 4.3 \times 10^5 M_{\odot}$, and the time cadence between outputs below $z = 2$ is 10 Myr.

Their bound masses agree relatively well at early times, to within $\approx 5\%$. However, their masses diverge after the subhalo becomes a satellite shortly after $z \approx 0.5$. Whereas HBT+ finds little to no change in its bound mass, the subhalo continuously loses mass in Subfind-HBT. This eventually leads to a 20% difference between both finders. The bound mass agrees between finders once it becomes a central again ($z \approx 0.3$), with the mass shooting up in just 10 Myr for Subfind-HBT. As soon as it becomes a satellite again ($z \approx 0.2$), the masses begin to diverge once more. It then undergoes a pericentre passage and mass is lost according to both finders, as expected from the effect of tidal stripping. By $z = 0$, the bound mass differs by 20%.

Through the evolution, the value of V_{\max} agrees much better between the subhalo finders. It remains constant after the initial growth of the subhalo, and only changes after the mass loss induced by tides at pericentre. As this quantity probes the inner part of the subhalo, the dichotomy between V_{\max} and M_{bound} tells us that mass is lost from the outskirts of the Subfind-HBT subhalo.

Indeed, this highlights one of the main differences between the two algorithms. Subfind-HBT finds (satellite) subhalo candidates within a FoF group by grouping particles that were bound to the same subhalo in the previous snapshot. The key difference relative to HBT+ is that Subfind-HBT does not account for particles that are re-accreted by satellites. In other words, particles may be found to be momentarily unbound at one output and then bound in the next. In HBT+, this is dealt with by associating more particles to a subhalo than those that are bound (see Han et al. 2012 for a discussion of why this is required). The approach that Subfind-HBT uses means that any particle that is found momentarily unbound will no longer be associated to that subhalo. Over time, this results into the outer layers of mass ‘evaporating’. As soon as the subhalo becomes a central, the method of candidate finding changes, and the missing mass is found once again. Despite the disagreement in the bound mass between Subfind-HBT and HBT+, it is easy to see that the tracking of both is better than Subfind, particularly during the pericentric passage at $z \approx 0.1$.

The differences in the bound mass evolution propagate to summary statistics. We show the cumulative bound mass function of satellites for the zoom-in simulation in Fig. B2. Subfind and Subfind-HBT agree well with each other, as found in the Gadget-4 release paper (Springel et al. 2021). However, they are both suppressed relative to what HBT+ finds. There is a weak mass dependence, with a 90% agreement at the lowest masses and 80% at the highest masses. We note that these differences should not be directly compared to those found in Fig. 6. In the version discussed in the main text, a fixed M_{bound} is made up by contributions from the satellite systems of centrals with different M_{200c} values. Here, we only consider a single FoF group of $M_{200c} \approx 10^{12} M_{\odot}$. Since Subfind struggles with major mergers (Fig. 12), the current dynamical state of haloes is clearly important in determining how well it recovers the satellite population. As zoom-in simulations generally target isolated haloes at $z = 0$, their selection may not be representative of the merger rates of haloes with similar masses (e.g. Genel et al. 2009).

Finally, other differences exist between HBT+ and Subfind-HBT. There is no hierarchy of subhaloes within FoF groups in

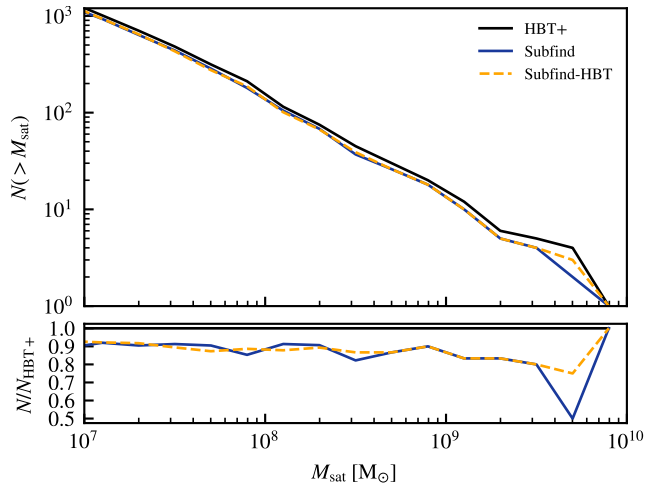


Figure B2. The cumulative bound mass function of satellite subhalos around a $M_{200c} = 10^{12} M_{\odot}$ halo. It was measured using HBT+, Subfind and Subfind-HBT. The ratios relative to HBT+ are shown in the bottom panel. Despite the history-based approach of Subfind-HBT, it is in closer agreement with Subfind than with HBT+.

Subfind-HBT. This helps improve parallelisation, as unbinding does not need to be done in a depth first approach. However, this means that mass stripped from satellites always ends up in the central subhalo, rather than possibly being accreted by its immediate parent. No phase-space checks are done between subhaloes, no hostless subhaloes exist and Subfind-HBT does not subsample particles during the unbinding of subhaloes and iterates until the number of bound particles has converged (similar to Subfind). In summary, these similarly named algorithms should be treated as different approaches to history-based halo finding.

APPENDIX C: DIFFERENCES IN VIRIAL MASSES

In §4.2.1 we showed the M_{200c} mass functions measured using different subhalo finders in the DMO and hydrodynamical versions of the simulations we analyse. Compared to HBT-HERONS, VELOCIRAPTOR and ROCKSTAR show systematic differences beyond the 1%-level across all the resolutions we consider in this study. We attributed these differences to miscentering in VELOCIRAPTOR and the different central definition in ROCKSTAR.

To show that this is the case, we match central subhaloes across subhalo finders. This approach allows us to identify whether any systematic differences exist in the properties of centrals, identified by any two subhalo finders. We perform the bijective matching as follows. We first match central subhaloes in catalogue A by identifying which subhalo in catalogue B contains the largest share of its bound particles. We then do the matching in reverse, i.e. from catalogue B to catalogue A, and only keep consistent matches. For the purposes of this discussion, catalogue A refers to the HBT-HERONS catalogues

In Fig. C1 we show the M_{200c} ratio of matched central subhaloes in the DMO L1_m9 simulation, as well as the spatial offset between their centres. The majority of centrals have similar M_{200c} values, even when the spatial offset is large. By visually inspecting several examples, we conclude that these occur whenever two similar mass subhaloes are interchangeably identified as centrals. Leaving aside these cases, there are outliers when matching across subhalo finders.

The most prominent outlier population occurs when matching to VELOCIRAPTOR, whose M_{200c} are underestimated by up to one order

of magnitude. By imaging the matches which disagreed the most in their M_{200c} values, we see that the underestimate is due to the centre being placed on a satellite, rather than on a central. As the centre of the aperture is not adequately positioned on the true peak of the overdensity, the R_{200c} is smaller and encloses less mass.

Some differences still remain when comparing to Subfind and ROCKSTAR. In particular, there are central subhaloes with large spatial offsets (≥ 200 kpc) that have more or less mass within R_{200c} . The distribution is very slightly skewed towards higher M_{200c} values in Subfind, but appears more symmetric in ROCKSTAR. We imaged several examples and saw that the differences are caused by different central identifications within the same FoF group. Despite the disagreement by factors of 4 in some individual cases, Subfind and HBT+ agree within 1% in their M_{200c} mass function. As ROCKSTAR has a similar distribution as Subfind, the M_{200c} mass function would agree to the same level, were it not for the different number of centrals resulting from its different definition.

APPENDIX D: LINKING ONLY DM OR ALL PARTICLES

Running ROCKSTAR on hydrodynamical simulations is typically done in one of two ways. The linking can be done using all particle types or just the dark matter ones. As explained in §3, we link all particle types for the main study. To provide an idea of how this choice affects the results, we repeat the comparison of mass functions as shown §4.2.

We show the M_{200c} mass function found in both choices of how to run ROCKSTAR in Fig. D1, expressed relative to the value found by HBT-HERONS. The choice of linking using all particles vs only DM ones can alter the measured mass function between the two ROCKSTAR variations by 5% at high and intermediate masses. The overall lower masses when running on all the particles is due to the issues that were identified in the main text: ROCKSTAR is unable to find subhaloes, and the centres are offset from the true density peaks. Thus, similar to what happens in the VELOCIRAPTOR miscentering, this lowers the measured M_{200c} . The differences become increasingly large at the lowest masses.

APPENDIX E: DIFFERENT MASS DEFINITIONS

The main results of this work depend on being able to compute the properties of (sub)haloes as consistently as possible across subhalo finders. To do this for the M_{200c} masses of haloes, we load the centres of central subhaloes as given by each subhalo finder into SOAP, so that we use the same routine to find the corresponding spherical overdensity mass. However, each subhalo finder outputs their own internally-computed M_{200c} , which may not be the same as the SOAP-computed value we use in this work. As past studies have likely used the values provided by the subhalo finders themselves, we explore by how much the value of M_{200c} changes once we compute it within SOAP.

We show in Fig. E1 the M_{200c} mass functions based on the internally-computed values for each subhalo finder, and we normalise each by the corresponding mass function based on the M_{200c} computed within SOAP. Subfind and VELOCIRAPTOR are well within the 1% difference, which reflects the fact that they use a very similar approach to SOAP when computing M_{200c} . All three include all mass, bound and unbound, within a given aperture.

The mass function derived from the ROCKSTAR-computed M_{200c} is also in good agreement with the one based on using SOAP. The agreement is not expected a priori, as ROCKSTAR only includes particles

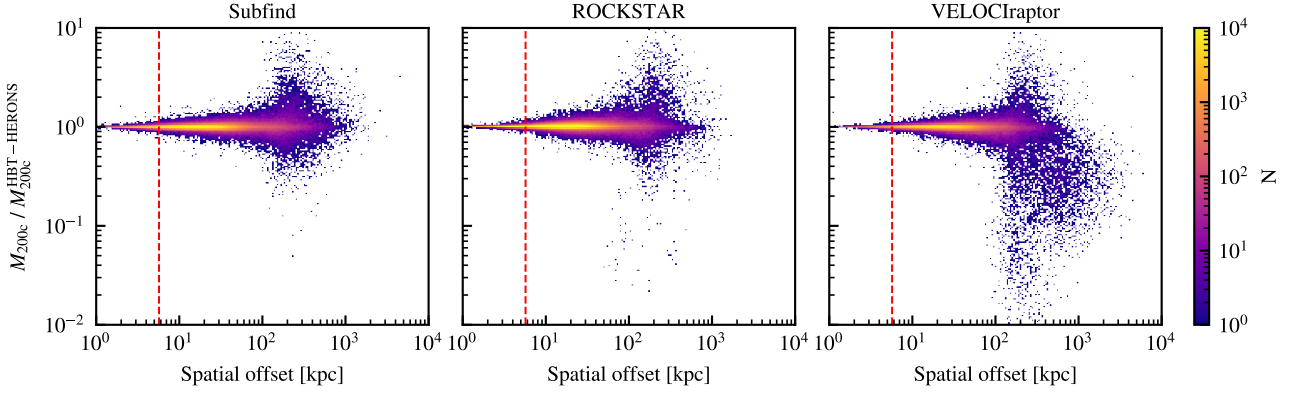


Figure C1. The M_{200c} values of haloes in the DMO L1_m9 simulation, measured in different subhalo finders and expressed relative to their matched counterparts found by HBT-HERONS. Only matched subhaloes identified as centrals by HBT-HERONS and with more than 100 particles enclosed within R_{200c} are shown. We limit the radial range to only show spatial offsets that are larger than those attributable to rounding errors. The vertical red line indicates the value of the gravitational softening length of the simulation at $z = 0$.

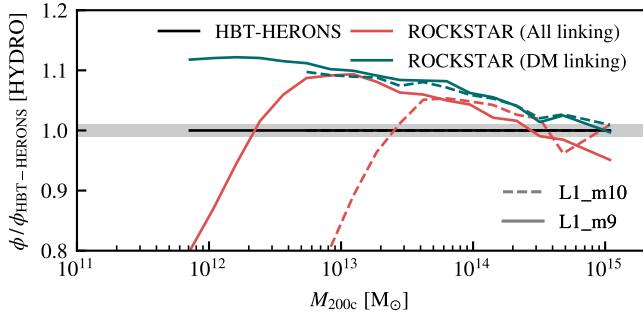


Figure D1. M_{200c} mass functions relative to those found in HBT-HERONS, for the hydrodynamical simulations used in this work. Two ROCKSTAR lines are present, which show how results change depending on how the 6D FoF algorithm is run. The red line is the method we used to run ROCKSTAR for the results shown in the main text, which does the 6D FoF finding using all particle types except for black holes. The teal line is an alternative approach that just uses the DM particles for 6D FoF finding and ignores the other particle types.

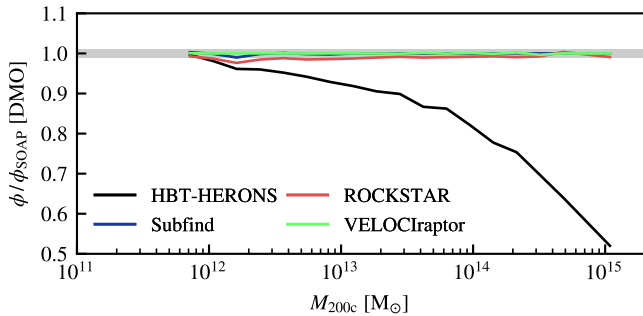


Figure E1. M_{200c} mass functions based on the values computed internally by each subhalo finder, relative to those computed by SOAP. The results are shown for the DMO L1_m9 simulation.

that are bound to the central, and so one might expect lower values relative to those measured in SOAP. However, a key choice made by ROCKSTAR reduces the differences between total and bound-only mass calculations. The bound mass is assigned inclusively, so the mass that is bound to satellite subhaloes may also be bound to central subhaloes. In practice this means that a large fraction of the

particles within R_{200c} end up formally bound to the central, at least according to the unbinding criterion used by ROCKSTAR. Hence, the differences in M_{200c} are minimal.

The M_{200c} mass function that changes the most is that based on the values provided by HBT-HERONS. Similar to ROCKSTAR, it only includes bound particles in its internal calculation. However, mass is assigned exclusively. This entails that mass bound to resolved satellites is not included within a given aperture. Consequently, the radius at which the mean enclosed density equals $200\rho_{\text{crit}}$ is smaller, and the mass enclosed within that physical radius is also less than when including the total mass. The extent of the effect depends on how many satellites are resolved, which is why the differences between HBT-HERONS and SOAP become larger as M_{200c} increases (i.e. as more particles sample the virial region of the halo).

The second change we made to ensure a more consistent comparison is to make ROCKSTAR assign masses to subhaloes in an exclusive manner. We do this because HBT-HERONS, Subfind and VELOCItaptor use an exclusive mass assignment, so ROCKSTAR-derived values for M_{bound} and V_{max} are systematically higher just because of this operational difference. The effect of this difference is clearly seen in Fig. E2, where ROCKSTAR has factors of 5 to 10 more bound mass for the highest mass central subhaloes compared to the exclusive mass version of Fig. 6. This change in definition also propagates to changes in V_{max} , as seen in Fig. E3.

To make ROCKSTAR work with exclusive masses, we modified its code so that particles can only be bound to a single subhalo. We make the internal change to the algorithm because including particles bound to other subhaloes during the unbinding step changes the overall gravitational potential, and hence the binding energies of particles. A simpler fix based on subtracting the mass bound to satellites from a given parent subhalo in post-processing would not account for the removal of additional gravitation potential contributed by particles already bound to satellites.

Leaving aside the practicalities of implementing exclusive or inclusive mass assignment, one may argue which of the two mass definitions is ‘best’. The dynamics in gravitational systems depend on the gravitational potential, regardless of whether the mass that sources it is formally associated to one object or another (or if it is not bound to any object, a possibility that none of the four subhalo finders we use here contemplate). One may therefore be inclined to use inclusive masses for V_{max} . However, inclusive masses can lead to double counting mass, if for example the stars of a galaxy are

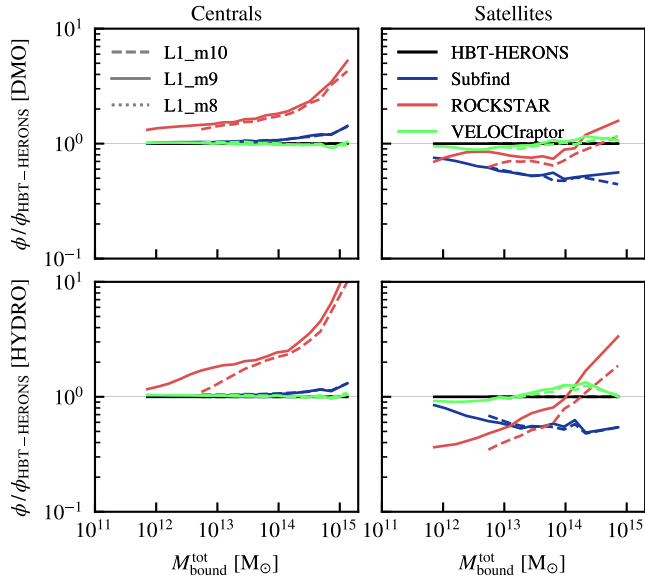


Figure E2. Same as in Fig. 6, but showing the results as provided by the default version of ROCKSTAR. As the masses computed by ROCKSTAR are inclusive, there is a systematic upwards shift in the number density at a fixed M_{bound} , as the other subhalo finders use exclusive mass definitions.

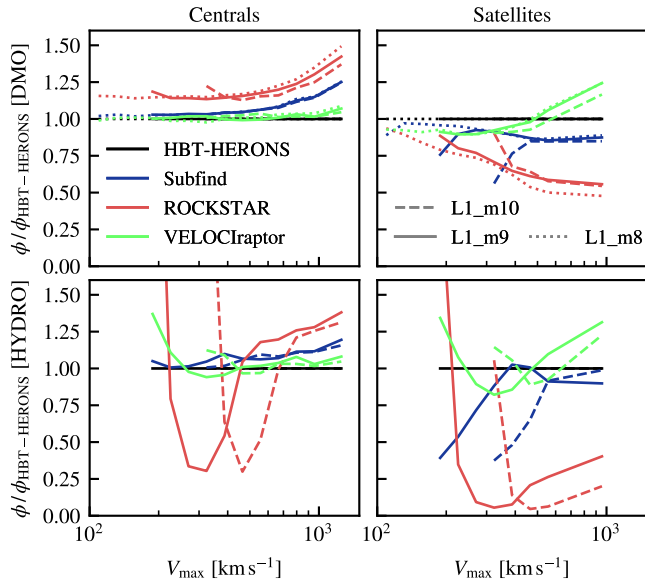


Figure E3. Same as in Fig. 8, but showing the results as provided by the default version of ROCKSTAR. As the masses computed by ROCKSTAR are inclusive, there is a systematic upwards shift in the number density of central subhaloes at a fixed V_{max} , as the other subhalo finders use exclusive mass definitions.

bound to both a satellite subhalo and its parent subhalo. This highlights that the choice of one definition should reflect the question one aims to answer. In any case, when making predictions to compare against the real Universe, this discussion is moot. Any, if not all, metrics we usually use to assign masses to (sub)haloes in simulations are theory-motivated and are not realistically measurable in the real Universe.

This paper has been typeset from a $\text{\TeX}/\text{\LaTeX}$ file prepared by the author.